A TECHNIQUE FOR THE PRODUCTION OF A HIGH AMPLITUDE, HIGH FREQUENCY, CONCENTRATED MAGNETIC FIELD FOR USE IN HYPERTHERMIA APPLICATIONS

Gareth Kevin Sessel

A dissertation submitted to the Faculty of Engineering and the Built Environment, University of the Witwatersrand, Johannesburg, in fulfilment of the requirements for the degree of Master of Science in Engineering.

Johannesburg, 2012

Declaration

I declare that this dissertation is my own unaided work. It is being submitted for the degree of Master of Science in Engineering to the University of the Witwatersrand, Johannesburg. It has not been submitted before for any degree or examination to any other university.

.....

(Signature of Candidate)

…… day of ……. …year …….

day *month* *year*

Abstract

Cancer of the liver is a common disease with a relatively poor prognosis. Hyperthermia is an exciting treatment that is under investigation. One modality of hyperthermia therapy makes use of an external magnetic field to produce losses in magnetic particles that have been supplied to the tumour. The losses result in the heating of the tumour cells thereby causing cell destruction. There exists a limit in the product of magnetic field intensity and frequency, above which eddy currents reach levels capable of causing thermal damage in healthy tissue. This limit is well documented in the literature and, due to the seriousness of the disease, can be increased to 5×10^9 A/ms.

The magnetic field used by most researchers is produced by simple coils. Using these simple coils, it is very difficult to produce sufficient heating throughout the tumour cells without exceeding the safety limit in healthy tissue. This research provides a machine that is capable of producing a magnetic field of sufficient energy to cause therapeutic heating within the tumour region whilst remaining within the safety limit elsewhere. A design methodology for this machine is demonstrated. A prototype machine is built and tested in order to validate the design procedure. The results from the prototype experiment are in good agreement with those predicted by the theory. The idea of "focussing" a magnetic field in distances far smaller than the wavelength of the field is a novel concept. This fundamentally new research has the potential to assist in the development of a treatment for tumour sufferers.

Acknowledgements

I would like to express my deep gratitude to Professor Ivan Hofsajer, my research supervisor, for his guidance, enthusiasm and useful critique of this work.

I would also like to thank Harry Fellows and Mark Goosens for their assistance in the construction of a prototype machine.

Finally, I wish to thank my parents, siblings, colleagues and friends for their support and encouragement.

CONTENTS

Nomenclature

Acronyms

AEH	Arterial Embolisation Hyperthermia
EMF	Electromotive Force
FEA	Finite Element Analysis
FP_1	Focus Pole Set 1
FP_2	Focus Pole Set 2
MMF	Magnetomotive Force
MMH	Magnetically Mediated Hyperthermia

Symbols

B	Magnetic flux density
E	Electric field
f	Frequency
H	Magnetic Field Intensity
θ_B	Magnetic flux
τ	Effective relaxation time
μ	Magnetic permeability
μ_0	Permeability of free space
μ_r	Relative permeability

Chapter 1

Introduction and Problem Description

1.1. INTRODUCTION

Despite a significant increase in the treatment options available to cancer sufferers, cancer remains a major problem in the medical industry. Cancer of the liver is a common and particularly problematic form of the disease [1]. The five-year survival rate is only 13% [2].

The objective of local hyperthermia treatment is to raise the temperature of the tumour to levels at which the tumour cells either initiate apoptosis (“cell-suicide”) or undergo necrosis. Ideally, the surrounding healthy tissue should remain below the safe maximum temperature limit and therefore be unharmed. This is appealing since the treatment would have far fewer side effects than other common treatments such as radiation or chemotherapy.

Common methods for reaching the elevated temperatures required for hyperthermia include the use of microwave, radiofrequency or ultrasound probes being placed directly into the tumour. These modalities suffer from setbacks such as the difficulty in targeting only the cancerous tissue thereby placing nearby organs at risk [3]. Additionally, they also tend only to heat the region of the tissue in which they are placed, thereby under-treating the tumour [3].

Magnetically mediated hyperthermia (MMH) may overcome these problems. It involves placing magnetic material throughout the tumour and using an externally applied magnetic field to heat the material using hysteresis losses, relaxation losses or eddy currents. There are different modalities of MMH. When discussing modality specific concepts (e.g. particle size), this dissertation will focus mainly on arterial embolisation hyperthermia (AEH). However, the primary contribution of this work is the magnetic field applicator. This may prove useful for all modalities of MMH. When fields are discussed within this dissertation, magnetic fields are implied.

In AEH, the blood supply to the tumour is used to deliver the magnetic particles and disperse them throughout the tumour region. The magnetic particles are supplied directly to the tumour using a catheter and radiologic guidance. This is particularly suited to the treatment of hepatic cancers, since the majority of their blood supply is obtained from the hepatic arterial system, whereas the healthy hepatic tissue obtains the majority of its blood supply from the portal venous system [4].

This makes it possible to place the required quantity of particles into the tumour whilst having a very low number of particles in the healthy liver tissue. AEH should result a tumour-wide distribution of the magnetic particles thereby simplifying the achievement of the required temperature distribution throughout the tumour [5].

Difficulties often encountered with AEH are related to the need to produce sufficient heating whilst using the least amount of magnetic particles possible. This is desirable since excessive particles have a toxic effect on the patient. The particles therefore must be highly biocompatible and exhibit high loss powers at the frequency and field amplitude of the magnetic field. Additionally, high frequency magnetic fields induce eddy currents in conductive materials. Eddy currents are therefore induced in the body of the patient i.e. in healthy tissue. If these are sufficiently large, they cause tissue heating and nerve/muscle stimulation [6]. The magnetic field present in healthy tissue must therefore be below a safe limit to avoid the damaging effects of large eddy currents.

Much of the research being done in the field of AEH consists of the design and characterisation of the magnetic particles to be supplied to the tumour. The magnetic fields used by the majority of the researchers are produced by a simple coil. Evidently, the need for a more sophisticated method for producing the required magnetic field has been underestimated and therefore overlooked. The proposed research will investigate the possibility of creating a magnetic field that is focusable, resulting in a high field amplitude within the tumour region and a field amplitude within the safety limits elsewhere.

This chapter provides background information regarding MMH. Problems facing other researchers in the field are presented. The contribution of this work is explained and the difficulties to overcome are stated and discussed in terms of physics.

1.2. PROBLEMS WITH NON-INVASIVE HYPERTHERMIA AS A CANCER TREATMENT

The most important and obvious requirement for hyperthermia treatment is the production of sufficient heat to achieve the desired temperature range throughout the tumour region. In order to accomplish this, the concentration of magnetic particles must be high enough and the magnetic field must have a sufficiently large amplitude and frequency. It is clear that losses increase with particle concentration, frequency and field amplitude.

1.2.1. Limitations of Magnetic Particle Concentration

The type of magnetic particle is chosen based on its biocompatibility. It must have a known toxicity that allows for the calculation of a safe dosage based on the body weight of the patient. However, even if dosages are used that are supposedly safe, high concentrations of the particles too close to major blood vessels could produce dangerous results in patients with impaired hepatic function [7]. The dose being given to the patient should therefore be as low as possible [8].

1.2.2. Limitations of the Magnetic Field

There are biological reasons to limit the maximum frequency and amplitude of the magnetic fields. If these limits are exceeded, the induced eddy currents may produce sufficient heat to damage healthy tissue. Additionally, induced voltages may give rise to nerve/muscle stimulation [6]. The typically accepted value for the maximum product of magnetic field intensity and frequency is 4.85 x 10^8 A/ms [6]. This figure was obtained in an experiment that placed a human subject within a 30cm diameter coil and varied the frequency and field amplitude until a value was reached for which the subject could remain in tolerable discomfort for more than one hour [6]. Due to the seriousness of the disease, some temporary patient discomfort can be tolerated in order to achieve the therapeutic effects of the treatment. The product of field amplitude and frequency can therefore be increased to 5 x 10^9 A/ms [6]. The objective of this research is to produce a magnetic field that is strongest within a small area (the tumour) whilst sufficiently weaker elsewhere. This would minimise the patient's discomfort and maximise treatment efficacy.

1.2.3. Difficulty in Achieving Heating throughout Tumour

It can be seen from sections 1.2.1 and 1.2.2 that there are good reasons to limit the particle concentration, field amplitude and frequency. However, since these properties are essential in achieving the desired therapeutic temperatures, limitations may prove problematic. There are two methods to overcome this problem. The first method is the focus of many researchers in this field. This method aims to produce magnetic particles with very large specific loss powers (SLP) i.e. particles that are more effective in converting the energy from the externally applied magnetic field into heat. Some researchers have made significant progress in this field. However, the SLP of these particles varies greatly with particle size, shape and microstructure [8]. It is therefore required that the particles be produced with very narrow distribution in terms of size and shape. This makes it difficult to manufacture these particles on a large scale.

The second method by which this problem may be overcome is to realise the possibility of a non-constant field amplitude. The objective of this approach is to create a magnetic field with flux lines that are highly concentrated in the area of the tumour but significantly less concentrated elsewhere. This would limit the generation of eddy currents in healthy tissue to the allowed amount, whilst any eddy currents in the tumour may exceed the allowed limit without negatively affecting the healthy tissue. Furthermore, in some cases, the full hysteresis loop of a material cannot be used due to the constraints on field amplitude [8]. Therefore, focussing the field may enable for the full loss powers of these particles to be realised. These materials may turn out to be superior to others if allowed to reach saturation flux densities [8].

1.3. MAGNETISM REVIEW

A detailed understanding is required, of the mechanisms that cause losses when magnetic materials are placed in an alternating magnetic field. An in-depth knowledge of magnetism allows for a good understanding of the problem and assists in the optimisation of the magnetic field in order to achieve maximum losses. This review is given in chapter 2.

1.4. PARTICLE OPTIONS

1.4.1. Commonly Used Materials

The materials used for MMH are typically magnetite (Fe_3O_4) or maghemite (γ-Fe_2O_3). These materials exhibit low toxicity and may give rise to particles with high loss powers [9]. These particles exhibit ferrimagnetism or superparamagnetism depending on particle size and temperature.

1.4.2. Particle Size

Particles used in AEH are delivered to the arteries that supply blood to the tumour. They must then flow freely in the arteries until they reach the capillaries at which point they must get stuck. This aims to place high concentrations of particles in the cells of the tumour. The size of capillaries varies on average between 5 μm and 10 μm [10]. Particle size must therefore be larger than 10 μm. A similar process is used for lung perfusion scans in which Technetium TC-99M Albumin Aggregated (99M TC-MAA) particles are trapped in the capillaries of the lung for imaging purposes. The particles used for this procedure are typically between 10 μm and 50 μm in diameter [10]. This is the same desired size range for the particles to be used in this project. This is an important consideration because particle size directly affects the loss mechanism, which is exploited to produce hyperthermia in the tumour cells.

1.4.3. Loss Mechanisms

The processes by which heating may occur can be split into four main categories. These are eddy current losses, resonance losses, hysteresis losses and relaxation losses. Particle heating by induced eddy currents can be neglected due to the microscopic size and low electrical conductivity of the particles [8]. Resonance losses can also be neglected since these occur at frequencies far higher than those suitable for therapeutic hyperthermia. Hysteresis is the predominant loss mechanism in multi-domain particles below the Curie temperature of the material i.e. corresponding to the ferrimagnetic behaviour of the material. Relaxation losses occur due to a combination of Néel and Brownian Relaxation [9]. Relaxation losses correspond to the superparamagnetic regime and are relevant in MMH when the particles consist of single domain nanoparticles, usually smaller than 20 nm in diameter [8]. When nanoparticles of the magnetic material are used, they are generally coated in a stable material to reach the dimensions necessary for the particles to become trapped in the capillaries of the tumour. Coating the particles also prevents agglomeration and protects the particles from the harsh environments often found in tumours and in the body in general.

1.5. MAGNETIC FIELDS

1.5.1. Difficulties in Focussing a Magnetic Field

1.5.1.1. The Principle of Minimum Total Potential Energy

The energy density of a magnetic field is given by equation 1.1 [11].

$$\text{energy density} = \frac{B^2}{2\mu} \qquad (1.1)$$

The principle of minimum total potential energy states that if a closed, stable system reaches equilibrium, its energy will be as small as possible. From equation 1, it can be seen that the energy is related to the flux density. Therefore, the flux lines will tend to spread out in order to minimise the flux density thereby minimising the energy of the system.

1.5.1.2. Gauss' Law for Magnetism

It is important to realise the importance of the Maxwell equation commonly referred to as Gauss' law for magnetism, which is given in equation 1.2.

$$\nabla . \mathrm{B} = 0 \qquad (1.2)$$

Equation 1.2 implies that magnetic flux lines have neither a beginning nor an end. If it were possible to terminate the magnetic flux lines on the area of interest – this would result in automatic focussing. Gauss' law for magnetism does not allow for this to occur. Instead, the flux lines will follow a return path, spreading out as they do so.

1.5.1.3. Antenna Array Theory

The focussing of a magnetic field in the far-field is possible using an array of antennas, each having an input of different amplitude or phase. Most array systems make use of the far-field assumption which approximates a spherical wave-front as a plane wave. For this to be valid, the distance between the antenna and the focal point must be large relative to the wavelength of the signal. Some near-field array theory does exist. However, it still requires a minimum distance between the antenna and the focal point and between the antennas in the array. If those distances are insignificant, relative to the wavelength, beam-forming using array theory is not possible.

In MMH, the wavelengths used are in the range of 1 km in length. The air-gap that is used to accommodate the patient, whilst sustaining a suitable amplitude of magnetic field intensity is several orders of magnitude smaller than this. Furthermore, the magnetic field applicator can make use of coils spaced very close together (< 1 cm if required). Under these conditions, antenna array theory is not a viable solution.

1.5.2. Proposed Solution

For this dissertation, simulations have been carried out for various configurations using the finite element analysis (FEA) software package, FEMM. The simulations have shown that it is indeed possible to increase the concentration of flux lines in a certain area. This has been achieved using additional coils to produce flux lines that destructively interfere with the flux in areas where low flux density is desired. Automated optimisation of the machine design allows for a design procedure to be formulated. The design process is described in chapter 3.

1.5.3. Experimental Verification

Once a final design for the machine was obtained, the scalability of the system was investigated. When a good understanding of this scalability was obtained, a small-scale machine was fabricated. Experiments on the small-scale model were performed and the experimental results were compared to the simulated results. This process is documented in chapter 4.

1.6. DRIVING ELECTRONICS

The machine is required to produce high field strengths at high frequencies. Frequencies in the range of 400 kHz to 500 kHz have been found to be useful in MMH applications [12]. The electronics should therefore be able to supply high currents at frequencies between 400 kHz and 500 kHz. Achieving such a system is not trivial. The construction of the electronic driving circuitry was required for the previously mentioned experiment. A description of the electronics is provided in chapter 4.

1.7. CONCLUSION

MMH has the potential to revolutionise the treatment of hepatic tumours. This is only possible if the problem of achieving the required heating, using reasonable quantities of magnetic materials, is overcome. A commonly overlooked area in MMH research is the advancement of the equipment that produces the magnetic field. No existing work, attempting to focus a magnetic field in an area in the very near-field, has been found. This dissertation attempts to put forward the first design procedure for such a system. This would be a highly beneficial contribution to the development of MMH as a viable cancer treatment.

REFERENCES

[1] Mayo Clinic staff, *Liver Cancer*, Mayo Foundation for Medical Education and Research, http://www.mayoclinic.com/health/liver-cancer/DS00399, last accessed 12 April 2011

[2] Cancer.Net, *Liver Cancer: Statistics*, American Society of Clinical Oncology, http://www.cancer.net/patient/Cancer+Types/Liver+Cancer?sectionTitle=Statistics, last accessed 12 April 2011

[3] Moroz P., Jones S.K., Gray B.N., *Magnetically mediated hyperthermia: current status and future directions*, Centre for Applied Cancer Studies, University of Western Australia, Perth, Australia, 2002

[4] Xu R., et al, *Three Dimensional Model for Determining Inhomogeneous Thermal Dosage in a Liver Tumor During Arterial Embolization Hyperthermia Incorporating Magnetic Nanoparticles*, IEEE Transactions on Magnetics, Nanjing, China, 2009

[5] Moroz P., Jones S.K., Gray B.N., *Tumor Response to Arterial Embolization Hyperthermia and Direct Injection Hyperthermia in a Rabbit Liver Tumor Model*, Journal of Surgical Oncology, 2002

[6] Hergt R., Dutz S., *Magnetic particle hyperthermia – biophysical limitations of a visionary tumour therapy*, Journal of Magnetism and Magnetic Materials, Germany, 2007

[7] Moroz P., et al, *Arterial embolization hyperthermia: hepatic iron particle distribution and its potential determination by magnetic resonance imaging*, Physics in Medicine and Biology, 2002.

[8] Hergt R., et al, *Physical Limits of Hyperthermia Using Magnetite Fine Particles*, IEEE Transactions on Magnetics, 1998

[9] Pavel M., et al, *Study of the Optimum Dose of Ferromagnetic Nanoparticles Suitable for Cancer Therapy Using MFH*, IEEE Transactions on Magnetics, Romania, 2008.

[10] Rhoades R., Bell D.R., *Medical Physiology: Principles for Clinical Medicine*, 3rd Edition, Lippincott, Williams & Wilkins, 2009

[11] Serway R.A., Jewett J.W., *Physics for Scientists and Engineers*, 6th Edition, Brooks Cole, 2003

[12] Hergt R., Dutz S., Zeisberger M., *Validity Limits of the Néel Relaxation Model of Magnetic Nanoparticles for Hyperthermia*, Nanotechnology, 2009

Chapter 2

Physics of Magnetism

2.1 INTRODUCTION

Magnetism plays an important role in magnetically mediated hyperthermia treatments. As a result, much effort has been made to understand the influencing factors of magnetic theory in order to exploit them for medically beneficial purposes.

In MMH, ferromagnetic, ferrimagnetic and superparamagnetic materials are commonly used. The hyperthermia effect is caused by losses in the magnetic materials, which can be attributed to several different loss mechanisms.

At particle sizes sufficiently large to accommodate multiple magnetic domains, magnetic hysteresis is the primary loss mechanism responsible for the therapeutic heating. When sufficiently small nanoparticles are used, each containing a single magnetic domain, they behave superparamagnetically. Losses in superparamagnetic particles are caused by relaxation effects.

This chapter describes magnetic theory in terms of physical principles in order to obtain insight into the mechanisms involved in AEH as discussed in this dissertation. Categories of magnetic materials are briefly described. An overview of the loss mechanisms is given. Explanations are given qualitatively rather than delving deep into a mathematical evaluation of current magnetic models. This section is therefore not intended as a detailed, quantitative investigation of magnetic phenomena.

2.2. BACKGROUND

A magnetic field is set up whenever there is electrical charge in motion. This can be the result of an electrical current in a conductive material [1]. If a magnetic field exists in a medium, then there will be magnetic flux. A rate of change of magnetic flux generates an EMF if the flux passes through a closed path. The unit of measurement for magnetic flux is the weber. One weber is defined as the amount of flux which, when decreasing to zero weber in one second, produces an EMF of 1 volt in a single turn coil enclosing the flux [1].

The intensity of the magnetic field, or the magnetic field strength H, can be understood as follows. An H value of 1 A/m can be found at the centre of a circular coil consisting of 1 turn, with diameter 1 m and with 1 A current flowing through it. This definition will become self-apparent when the Biot-Savart law is applied to a single coil geometry. This is described below.

The intensity of a magnetic field, H, resulting from an electric current flowing in a conductor can be calculated using the Biot-Savart law, shown in equation 2.1 [1].

$$\Delta \boldsymbol{H} = \frac{1}{4\pi r^2}\, i\, \Delta \boldsymbol{l} \times \boldsymbol{u} \qquad (2.1)$$

where *i* is the current flowing in a length Δ*l* of a conductor, r is the radius of the conductor and **u** is a unit vector parallel to the radial direction.

2.2.1. Magnetic Field in a Coil

Equation 2.1 can be used to calculate the field intensity at the centre of a single turn coil. By dividing the coil into arcs and summing their contributions at the centre of the coil, it can be found that the field intensity within the centre of the coil is:

$$\boldsymbol{H} = \frac{i}{2r} \ {}^{A}/_{m} \qquad (2.2)$$

2.2.2. Magnetic Field in a Solenoid

A simple device for achieving a uniform magnetic field is a solenoid. In the case of an infinitely long solenoid, the field intensity throughout the solenoid is given by equation 2.3.

$$\boldsymbol{H} = \frac{Ni}{2\pi r} \ {}^{A}/_{m} \qquad (2.3)$$

where N is the total number of turns in the solenoid.

2.2.3. Relationship between Field Intensity (H) and Flux Density (B)

If a current produces a magnetic field H in a material (or free space), magnetic flux will exist in that material. As a result, there will be a flux density, B (a.k.a. magnetic induction). This will occur regardless of the material and the magnitude of the flux density will depend on the field intensity H, and the permeability of that material.

There is a relationship between the magnetic field intensity H and the flux density B. The two quantities are related to each other by the permeability of the medium in which the magnetic flux exists. This relationship can be seen in equation 2.4.

$$B = \mu_r \mu_0 H \qquad (2.4)$$

where μ_0 is the permeability of free space and μ_r is the relative permeability of the material. The relative permeability describes how the flux density in a material differs from that in free space, for a given field intensity.

In free space, equation 2.4 reduces to:

$$B = \mu_0 H \qquad (2.5)$$

Equation 2.5 shows that in free space, the relationship between B and H is always linear. Therefore, if H is known and the medium is free space, then B is easily obtainable and linearly related to H. For this reason, whilst analysing the field values in free space, H and B have been used interchangeably. If focussing is shown using H, identical focussing will occur in B.

μ_r in equation 2.4 is not always a constant value and can vary with the field intensity. The exact value for a given magnetic field and medium can be obtained from the gradient of the magnetisation curve for that medium, at the specific field intensity.

2.2.4. Faraday's Law of Induction and Lenz's Law

Faraday's law of induction states that voltage induced in an electrical circuit is proportional to the rate of change of magnetic flux in the circuit. Lenz's law states that this induced voltage will be in a direction which will oppose the flux that produced it. A consequence of these laws is that conductive materials, placed within the alternating magnetic field, can be used to block the inducing magnetic flux. This consequence is used advantageously in the machine design stage to create magnetic shields. This is documented in chapter 3.

2.3. MAGNETIC MOMENTS AND MAGNETISATION

In order to develop an understanding of the different magnetic material classifications, it becomes important to look at the effect that a material has on the magnetic field. Additional properties that require investigation are the magnetic moment, magnetisation, susceptibility and remanence.

A magnetic moment is a vector quantity that describes the torque on a magnetic system (such as a dipole or current loop). A magnetic moment of one $A.m^2$ experiences a maximum torque of one N.m when its orientation is perpendicular to that of magnetic flux density of one tesla. This explanation suggests that the magnetic moment will try to align itself parallel to the flux density B.

Magnetisation can be defined as the magnetic moment per unit volume of a solid medium. Magnetic moments and magnetisation will be used throughout the remainder of this chapter to describe other magnetic phenomena.

2.4. CLASSIFICATION OF DIFFERENT MAGNETIC MATERIALS

2.4.1. Diamagnetism and Paramagnetism

The magnetic properties of diamagnetic and paramagnetic materials, at room temperature, are very weak and neither displays hysteresis [2].

Diamagnetic materials are made up of atoms with a net magnetic moment of zero [2]. When a diamagnetic material is placed in a magnetic field, moments are induced in the atoms which, according to Lenz's law, oppose the field that induced them. This results in diamagnetic materials' having a relative permeability slightly lower than one.

Paramagnetic materials are made up of molecules with magnetic moments of constant amplitudes. When placed in a magnetic field, the magnetic moments of the molecules (of the paramagnetic material) will experience a torque which will try to align them with the magnetic field, thereby producing a non-zero, net magnetic moment per unit volume of material i.e. magnetisation [2]. At a temperature of absolute zero, the magnetic moments would align completely with the magnetic field resulting in the achievement of the maximum possible magnetisation. This is called the saturation magnetisation, M_s. In contrast to diamagnetic materials, paramagnetic materials have relative permeabilities slightly greater than one.

Any significant amount of materials which make up the human body are either diamagnetic or paramagnetic [3]. Additionally, copper is a paramagnetic substance. In practice, even though the relative permeabilities of these materials differ slightly from unity, they can be assumed to be unity in the case of a medical hyperthermia system. For this reason, the body of the patient is assumed to not influence the magnetic field output by the machine in any way. Additionally, when copper shields are placed in the machine (as described in chapter 3), its non-unity relative permeability is

ignored. In comparison to the material that makes up the machine, the relative permeabilities of the human body as well as of the copper can be neglected.

2.4.2. Ferromagnetic, Antiferromagnetic and Ferrimagnetic Materials

Ferromagnetic materials have a large net magnetisation, persisting without the presence of an external magnetic field. This is caused by the parallel alignment of the magnetic moments from each atom.

Ideal, antiferromagnetic materials have a net magnetisation of zero. This is caused by the antiparallel alignment of the magnetic moments from each atom, which sum to zero. In real materials and temperatures greater than 0K, a small net magnetisation will be present.

Ferrimagnetism is a special case of antiferromagnetism, in which the magnetic moments on the sublattices are in opposite direction but there is a net magnetisation. This is a result of the magnetic moments not being equal in magnitude, thereby causing a net magnetic moment. The magnetic moments in crystals of ferromagnetic, antiferromagnetic and ferrimagnetic materials are shown in Figure 1.

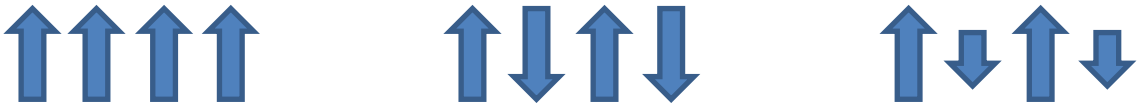

(a) (b) (c)

Figure 1: Magnetic moments in a: (a) ferromagnetic crystal, (b) antiferromagnetic crystal and (c) ferrimagnetic crystal.

This result explains the similarity between ferrimagnetism and ferromagnetism, since both have spontaneous magnetisations at room temperature. The magnetisation curves for the materials are also similar, with both ferrimagnets and ferromagnets exhibiting hysteresis and saturation [1]. Even though there is a net magnetisation, the saturation magnetisation of ferrimagnetic materials is generally significantly lower than that of ferromagnetic materials. Ferrimagnetic materials have very low conductivities and as a result support very little eddy currents [2]. They are frequently used in high frequency magnetic applications and are commonly referred to as ferrites.

The energy, which causes the alignment of the magnetic moments, is called exchange energy [1]. The magnetic exchange energies of the materials discussed above are very large. However, if the temperature of the material is raised high enough, thermal energy becomes large enough to

overcome the exchange energy. When this occurs, the coupling causing the alignment of the magnetic moments is destroyed and the magnetic moments align in a random manner. The temperature required to overcome the exchange energy is known as the Curie temperature, above which the magnetisation is zero. This is due to the vector summation of the randomly oriented magnetic moments, which will equal zero. Both ferromagnetic and ferrimagnetic materials lose their magnetisations at their Curie temperatures. When these materials exceed their Curie temperatures, they behave as paramagnetic materials.

This property is often exploited in medical hyperthermia systems as it allows for self-regulating particles or seeds i.e. the particles will not have hysteresis losses if the temperature is greater than the Curie temperature, thereby capping the maximum temperature that the particles may reach.

Despite possessing spontaneous magnetisation, in a bulk quantity the magnetisation of a ferromagnetic or ferrimagnetic material is zero. When an external, magnetic field is applied, the material acquires a magnetisation far larger than that of the external field. This can be explained using magnetic domains. A magnetic domain encompasses a large number of atomic, magnetic moments. The orientations of the moments within the domain are aligned such that the magnetisation of the domain is almost saturated. Therefore each domain possesses the spontaneous magnetisation that is expected of a ferromagnetic or ferrimagnetic material. However, the direction of magnetisation varies randomly from one domain to the next, resulting in a net magnetisation of zero in a sample sufficiently large to have multiple domains. When an external magnetic field is applied, the domains tend to align themselves in a similar orientation, thereby producing the large net magnetisation for the bulk material.

The qualities of ferromagnetic and ferrimagnetic materials that are used throughout the experimental section of this work are now described.

2.5. IMPORTANT QUALITIES OF FERROMAGNETIC AND FERRIMAGNETIC MATERIALS

2.5.1. Permeability

One of the most important properties of ferromagnetic and ferrimagnetic materials is their high relative permeabilities. The permeability of a material can be obtained by examining the gradient of its magnetisation curve.

2.5.2. Retentivity, Remanence, Coercivity and Saturation Magnetisation

Retentivity is the ability of a ferromagnetic or ferrimagnetic material to retain its magnetisation after the external magnetic field is removed. The remanence is a measure of either the remaining flux density or magnetisation after the magnetic field has been removed after the magnetic material has reached saturation.

Coercivity is the intensity of the magnetic field, in the reverse direction, required to reduce the flux density (B) from saturation to zero. After the Curie temperature is reached, both the remanence and coercivity become zero. The material then behaves as a paramagnetic material.

Saturation magnetisation is the maximum magnetisation that a given material can achieve. It occurs when all the magnetic domains are fully aligned with the direction of the magnetic field intensity, H [1]. Figure 2 relates these quantities to the hysteresis curve.

2.5.3. The Hysteresis Curve

A convenient way to examine the bulk magnetic characteristics for a particular material (ferromagnetic or ferrimagnetic) is to examine the flux density (B) as a function of field intensity (H), over a continuous range of H. When examined for multiple cycles, the hysteresis curve is obtained. Important information can be obtained from the hysteresis curve. The axes intercepts provide information about the retentivity and coercivity of the material. This is shown in Figure 2. Additionally, the area enclosed by the curve can be used to obtain the losses experienced per unit volume of the material per cycle. In this section, it will be assumed that the temperature of the material is far below the Curie temperature.

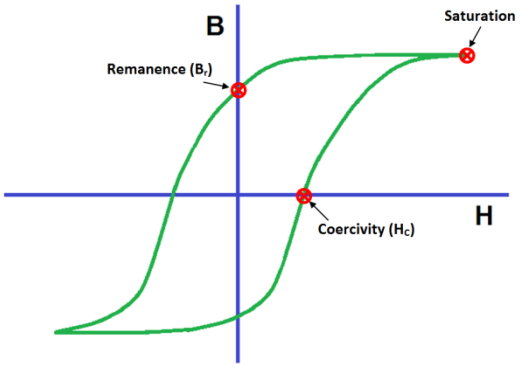

Figure 2: Hysteresis curve showing saturation flux density, flux density remanence and coercivity.

The coercivity, H_c, is equal to half of the distance between the two intercepts of the H axis. The point at which the curve cuts the B axis is the remanence B_r. The hysteresis loss per unit volume per cycle is equal to the area enclosed by the curve. This is shown in section 2.7.1.

2.5.4. Magnetocrystalline Anisotropy

Magnetocrystalline anisotropy is used to explain the dependence of a material's characteristics on the direction of magnetisation of a grain of the material. In an anisotropic solid, the magnetic moments will tend to align with specific axes within the crystal structure, since alignment with these axes mark minimum energy configurations [1]. When an external magnetic field is applied, the magnetic moments may be dislodged and re-align themselves with another axis in a new minimum energy configuration which is closer in alignment to that of the applied field's direction.

Magnetocrystalline anisotropy affects the values of coercivity and remanence and has a large impact on the shape and enclosed area of the hysteresis curve. Since it is this enclosed area that directly relates to the hysteresis losses (as explained in section 2.7.1), it can be understood that magnetocrystalline anisotropy contributes to the total hysteresis losses.

2.6. DOMAIN WALLS AND SINGLE DOMAIN GRAINS

The interfaces between individual domains in multi-domain grains are called domain walls. Domain walls are the transition layers that allow for a change in magnetic moment orientation from one domain to the next [1]. The width of a domain wall is a finite value that depends on the specific type of domain wall as well as the exchange and magnetocrystalline energies [1].

If the size of the grain decreases to a volume too small to accommodate a domain wall, the grain becomes a single domain particle. This transition occurs at a critical grain size, below which the grain exhibits spontaneous magnetisation since a single domain of ferromagnetic or ferrimagnetic material is magnetised to its saturation magnetisation. The critical grain size is dependent on multiple properties including the precise shape of the grain as well as the saturation magnetisation.

2.6.1. Superparamagnetic Particles

If the size of a single domain grain is decreased even further, another phenomenon is noticed in which the coercivity and remanence of the grain decrease to zero. This suggests the existence of an additional critical grain size, below which the grain becomes superparamagnetic.

The orientation of magnetisation of a single domain grain lies along the axis that offers a least energy configuration, as explained in section 2.5.4. In the microscopic realm, there is continuous fluctuation of thermal energy [4]. If the volume of the grain is small enough, such that the grain becomes superparamagnetic, the anisotropy energy becomes smaller than the thermal energy fluctuations. When this occurs, the fluctuations in thermal energy are sufficient to dislodge the magnetic moment from its axis, thereby changing the orientation of the magnetisation of the grain. If measured for a sufficiently long time, the observed magnetisation is an average value. This net magnetic moment, in the absence of an external field, appears to be zero. In the presence of an external field, the alignment of the magnetic moment will generate a behaviour similar to that of a paramagnetic substance. However, since the superparamagnetic grain consists of a large number of atoms (but a single domain), and the domain is magnetised to saturation, its susceptibility value is far higher than that of a standard paramagnetic substance.

2.7. LOSS MECHANISMS

There are conflicting opinions regarding the most effective loss mechanism to make use of for MMH. Experiments performed by Moroz have used coated iron-oxide particles, the centres of which were 100 nm to 200 nm in diameter [5]. These particles are produced specifically for AEH by Sirtex Medical and, at the above-mentioned dimensions, must rely on hysteresis losses to produce hyperthermia. In some materials, if the correct particle size is attained and sufficient field intensity is available, hysteresis losses are greater than losses by other mechanisms [6]. However, superparamagnetic particles are more likely to supply useful levels of heating at reduced magnetic field intensities [7]. Much research, on the application of both loss mechanisms, is being performed. Most research thus far, based on laboratory models and animal experimentation, have struggled to achieve suitable heating without significantly exceeding the safety limit of field intensity and frequency [7]. If this safety limit was obeyed, the level of hyperthermia achieved would likely be reduced to an inadequate amount, regardless of the loss mechanism in use. The focused magnetic field may overcome this limitation, thereby assisting in the development of a useful therapy. With this in mind, it is still important to have an understanding of the available loss mechanisms. These loss mechanisms will now be discussed.

2.7.1. Hysteresis

The area enclosed by the B-H curve is equal to the hysteresis losses per unit volume of material per cycle. From energy conservation, if a coil is wound around a magnetic material and energised, the energy will be stored or dissipated in the magnetic material.

Equation 2.6 describes the energy in such a system. V(t) is the potential difference across the terminals of the coil and *i*(t) is the current flowing through the coil.

$$E(t) = \int_0^t V(t)\, i(t)\, dt \qquad (2.6)$$

$$= Vol \times \int_0^B H(t)\, dB(t)$$

since $V(t) = NA\frac{dB(t)}{dt}$, $i(t) = \frac{H \times l}{N}$ and $l \times A = Vol.$

Cold working or adding non-magnetic elements into a material that exhibits hysteresis can increase the material's hysteresis loss and coercivity [1]. This suggests that these imperfections (dislocations or impure elements) give rise to an internal friction and are the root cause of the additional energy lost during each cycle of the magnetisation process [1]. An additional process that contributes to hysteresis losses is caused by magnetocrystalline anisotropy. The remainder of this discussion will attempt to provide an intuitive understanding on hysteresis losses.

In the initial magnetisation of a ferromagnetic or ferrimagnetic material, under the influence of a modest external magnetic field (low values of field intensity, H), the domains of the material that are nearly aligned with the direction of the external field stretch [8]. This is at the expense of the domains that are not aligned with the external field. This stage of the magnetisation process is reversible (region 1, Figure 3). If a sufficiently large field intensity is applied, the moments of the domains achieve enough rotation such that the flux density remains even when the external field is removed. This is caused by the re-orientation of the less favourably aligned magnetic moments. This corresponds to the inelastic section, region 2, of Figure 3. If the magnetic field intensity continues to increase, eventually all the magnetic moments will align with the external field. This is the cause of the saturation flux density. This is shown in region 3 of Figure 3. After the saturation flux density is reached, at higher values of H, the gradient of the B-H curve approaches that of free space i.e. μ_0 [8].

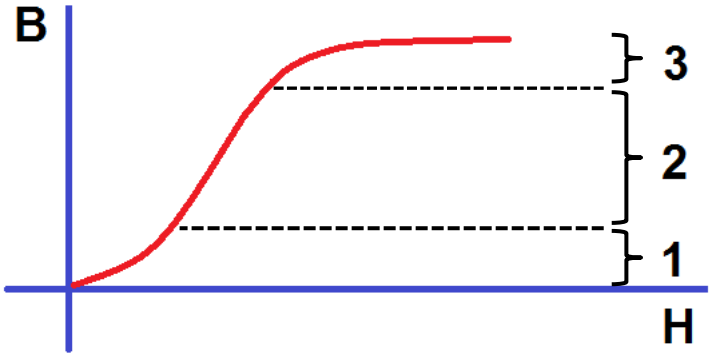

Figure 3: Initial magnetisation of ferromagnetic or ferrimagnetic material. The elastic, inelastic and saturation regions (regions 1, 2 and 3 respectively) are shown.

The energy, per unit volume, required to magnetise an initially unmagnetised sample of material is the grey shaded area in Figure 4a. The energy, per unit volume, returned when the external field is removed is equal to the green shaded area in Figure 4b. The difference between these energies is a result of the inelastic process and is dissipated in the form of heat. If the applied field is alternating, the full hysteresis curve is carried out per cycle and the area enclosed by the curve (green shaded area - Figure 4c) is equal to energy dissipated as heat (per unit volume) as described by equation 2.6 [8]. The total power dissipation from hysteresis losses is given by equation 2.7.

$$P = \int_V [\oint (H\, dB)]\, dV \qquad (2.7)$$

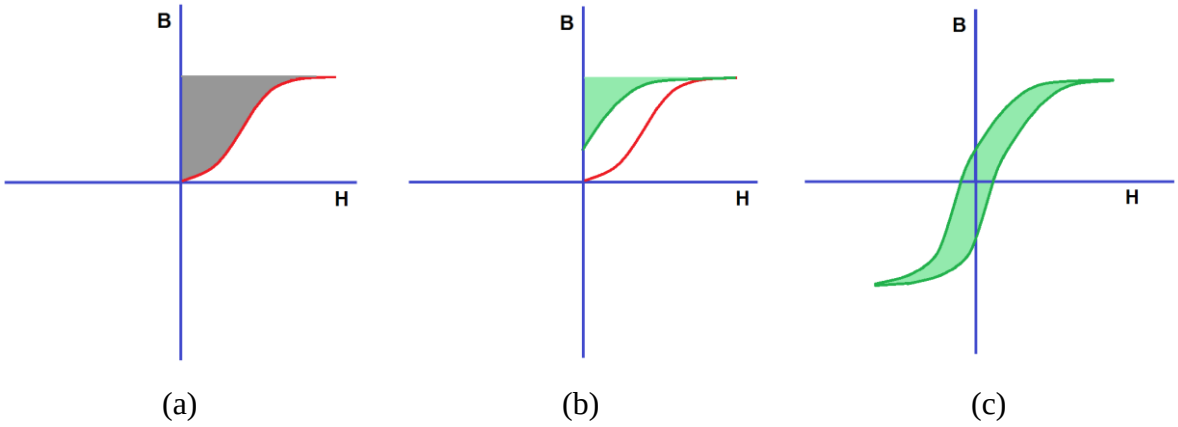

(a) (b) (c)

Figure 4: Energy dissipated as heat and energy recovered in a cycle of a hysteresis loop.

In many cases in MMH, the full saturation curve of the particles cannot be achieved. This is a result of the maximum limit of H x *f*, discussed in chapter 1. The field intensity, H, in MMH applications is often not large enough to saturate the magnetic material. The rated specific loss power (SLP) of a

material is of little use if the magnetic field is unable to adequately magnetise the material. This has provided additional complications to other researchers in the field [9]. This serves as additional justification for the development of a focussed magnetic field since the field intensity within the tumour region could be pushed high enough to saturate the magnetic material whilst remaining below the safety limit elsewhere.

2.7.2. Eddy Currents

According to Maxwell's Equations, a changing magnetic flux in a material induces an EMF in the material. In a conducting material, the EMF causes localised eddy currents to flow. This in turn produces heat through standard i^2R losses. Eddy currents are not a method of heating used in this work since the particles used are too small to support significant eddy currents. Additionally, the particles used are often ferrimagnetic and the conductivities of these materials are very low.

2.7.3. Néel and Brownian Relaxation

When a superparamagnetic particle is exposed to a high frequency alternating magnetic field, heat is produced from the reorientation of the magnetic moment of the particle. Thermal energy dissipation is caused either by the rotation of the particle within an encompassing viscous fluid (Brownian relaxation) resulting in frictional losses or by the rotation of the magnetic moment relative to the single domain grain (Néel relaxation) or a combination of both [10]. In the case of Néel relaxation, the thermal energy is dissipated when the magnetic moment of the particle relaxes to its lowest energy orientation [6]. Generally, the highest contributor when superparamagnetic particles are used is the relaxation mechanism with the shorter relaxation time [11]. The relaxation time is the mean time between two re-orientations of the magnetic moment. The combined power dissipation from Brownian and Néel relaxation losses is calculated using equation 2.8 [12].

$$P = k_r H_{peak}^2 f \frac{2\pi f\tau}{1+(2\pi f\tau)^2} \qquad (2.8)$$

where τ is the effective relaxation time and k_r is dependent on the permeability of free space, the susceptibility of the material and the magnetic field.

2.8. SUPERCONDUCTIVITY AND THE MEISSNER EFFECT

Superconductors are a class of materials whose electrical resistance drops to zero below some critical temperature. It is well understood that the potential difference across a conductive material is proportional to the electric field inside the material. From Ohm's law, it then follows that the electric field is also proportional to the resistance of the conductive material. In the case of a superconductor, the resistance equals zero (below the critical temperature). Therefore, the electric field in a superconducting material must be zero.

Equation 2.9 shows Faraday's law of induction [13].

$$\oint \boldsymbol{E}.d\boldsymbol{s} = -\frac{d\boldsymbol{\theta_B}}{dt} \qquad (2.9)$$

Where $\oint \boldsymbol{E}.d\boldsymbol{s}$ is the line integral of the electric field around a closed loop and $\frac{d\boldsymbol{\theta_B}}{dt}$ is the rate of change of magnetic flux through the loop.

From equation 2.9, it can be seen that if the electric field is zero (as it is inside a superconductor) then the change in magnetic flux is also zero i.e. the magnetic flux inside the superconductor remains constant.

When a superconductor is placed in a magnetic field (static or time varying), currents induced on its surface produce a magnetic field which is exactly equivalent in magnitude but opposite in phase to the external field. The magnetic field produced by the induced surface currents therefore entirely cancels the external field at the surface of the superconductor. This explains why magnetic flux does not pass through superconductors. It can therefore be seen that superconductors act as perfect magnetic shields. This property of superconductors is known as the Meissner effect and it is exploited in the design of the magnetic field applicator (chapter 3). Figure 5 shows the flux lines avoiding a superconducting sphere (a) and passing unperturbed through a conductive sphere (for non time-varying magnetic flux) (b). Ordinary conductive materials exhibit similar flux blocking characteristics when placed in a time varying magnetic field of sufficient frequency. This is shown in Figure 5(c). There is some flux penetration of the conductive sphere but it is clear that the flux is being partially expelled. This effect will be used for blocking flux in chapters 3 and 4.

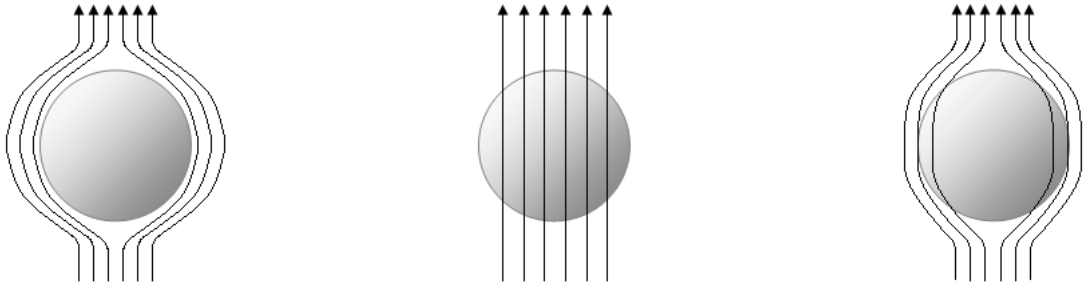

(a) (b) (c)

Figure 5: (a) Superconducting sphere excluding magnetic flux lines, (b) standard conductor being penetrated by non-time-varying magnetic flux lines and (c) time-varying flux lines (of sufficient frequency) being partially expelled by conductive sphere.

2.9. CONCLUSION

The understanding of magnetic phenomena is important when designing magnetic machines for MMH. Background information regarding the nature of magnetic fields has been discussed. The different classifications of magnetic materials have been stated and explained. These materials exist in the MMH system and must be understood in order to make intelligent design decisions. The losses in the magnetic materials, resulting from their exposure to an alternating magnetic field, have been described. It is these losses that are responsible for producing hyperthermia in the tumour cells. Finally, the ability of conductors to block flux was explained. This property proves to be very useful in improving the efficacy of the final machine.

REFERENCES

[1] Jiles D. *Introduction to Magnetism and Magnetic Materials*. Taylor & Francis Group, Florida USA, second edition, 1998.

[2] Della Torre E. *Magnetic Hysteresis*. IEEE Press, New Jersey USA, 1999.

[3] Kirschvink J L, Kobayashi-Kirschvink A, Diaz-Ricci J C, Kirschvink S J. *Magnetite in Human Tissues: A Mechanism for the Biological Effects of Weak ELF Magnetic Fields*. Bioelectromagnetics, suppl 1:101-13, 1992.

[4] Cullity B D, Graham C D. *Introduction to Magnetic Materials*. John Wiley & Sons, New Jersey, second edition, 2009.

[5] Moroz P., Jones S.K., Gray B.N. *Tumor Response to Arterial Embolization Hyperthermia and Direct Injection Hyperthermia in a Rabbit Liver Tumor Model*, Journal of Surgical Oncology, 2002

[6] Hergt R., et al. *Physical Limits of Hyperthermia Using Magnetite Fine Particles*, IEEE Transactions on Magnetics, 1998

[7] Pankhurst Q A, Connolly J, Jones S K, Dobson J. *Applications of Magnetic Nanoparticles in Biomedicine*, Journal of Physics D: Applied Physics, Vol. 36, pp R167-R181, 2003.

[8] Smith R J, Dorf R C. *Circuits, Devices and Systems*. John Wiley & Sons, New Jersey, fifth edition, 1992.

[9] Baker I, Zeng Q, Li W, Sullivan C R. *Heat Deposition in Iron Oxide and Iron Nanoparticles for Localized Hyperthermia*, Journal of Applied Physics, Vol 99, 08H106-08H106-3, 2006.

[10] Fortin J P, Gazeau F, Wilhelm C. *Intracellular Heating of Living Cells through Néel Relaxation of Magnetic Nanoparticles*, European Biophysics Journal. Vol 37, pp 223-228, 2008.

[11] Fannin P. C. and Charles S. W. *The Study of Ferrofluid exhibiting both Brownian and Néel Relaxation*, Journal of Physics D: Applied Physics, Vol. 22, pp 187, 1989.

[12] Rosensweig R E. *Heating Magnetic Fluid with Alternating Magnetic Field*, Journal of Magnetism and Magnetic Materials, Vol 252, pp 370–374, 2002.

[13] Serway R A, Jewett J W. *Physics for Scientists and Engineers*, 6th Edition, Brooks Cole, 2003

Chapter 3

Focussing the Magnetic Field

3.1. INTRODUCTION

The standard method for applying the time-varying magnetic field required for AEH is to place the patient in a basic solenoid [1]. The solenoid configuration is well documented and its characteristics are well known [2]. This is mentioned here in order to form a starting point upon which improvements can be made.

The magnetic field in an ideal, infinitely long solenoid is uniform over both the length and diameter of the solenoid [3]. Practically, however, the magnetic field varies according to the geometry of the specific solenoid. The solenoids typically used in magnetically mediated hyperthermia applications have large diameters relative to their lengths. This enables them to be placed around the body of a patient without occupying a significant length of the patient's body. The solenoid is used to generate the time varying magnetic field throughout a tumour-bearing region of the body. This technique has a serious drawback – all tissue in the region suffers from induced eddy currents [4]. This means that healthy tissue is in danger of thermal damage unless design considerations have been made. These considerations must ensure that the frequency and amplitude of the external field do not exceed certain limits.

A focussed magnetic field would allow for large field amplitudes within a tumour, allowing for less magnetic material to be placed within the liver whilst still achieving the temperatures required for successful treatment. This would be achieved without exceeding the safe operating limit in healthy tissue thereby ensuring that no damage to healthy tissue is caused.

As discussed in chapter 1, the focussing of a magnetic field in the near field is a difficult problem to overcome. The tendency of physical systems to occupy a minimum energy state as well as consequences arising from Maxwell's equations result in flux lines that tend to spread out. Furthermore, there appears to be a general lack of theory and previous results detailing this problem. This may be due to the fact that the usefulness of a focussed field has thus far been overlooked. Placing radiating elements in an array configuration does not produce the desired focussing if the target area is far closer than the wavelength of the fields used i.e. antenna arrays do

not perform in the very near field. The frequencies used are limited to 500 kHz as these are able to penetrate biological tissue entirely.

Section 3.2 of this chapter describes the success criteria i.e. the performance requirements of the focussed magnetic field in comparison to the field produced by a standard coil pair. Section 3.3 of this chapter aims to demonstrate the feasibility of a focussed magnetic field. The remainder of the chapter discusses constraints and design decisions and results in the formulation of a design procedure. Finally, conclusions are drawn.

3.2. BASELINE FOR COMPARISON

Before performing a detailed investigation on the design of the device used to produce a focussed magnetic field, it is necessary to have a good idea of what that field needs to outperform. As stated above, the magnetic field intensity within an ideal, infinitely long solenoid is constant i.e. no focussing takes place. If focussing is desired, it therefore becomes necessary to move away from the technique of placing the patient within a solenoid. Instead, a magnetic field oriented perpendicular to the body is chosen for this investigation. Consider the configuration shown in Figure 6.

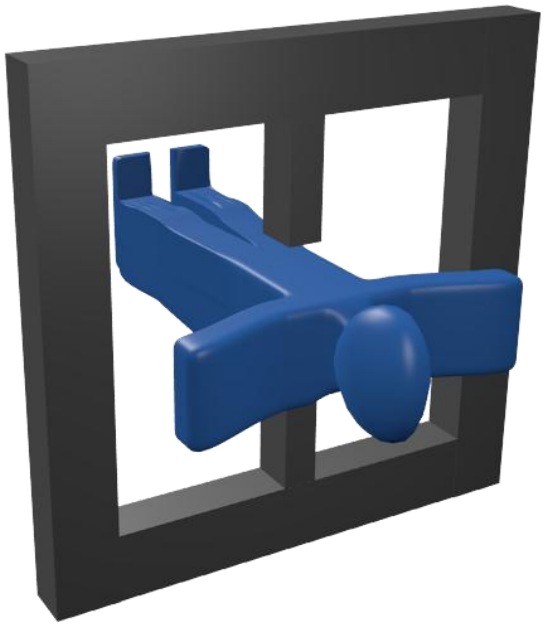

(a)

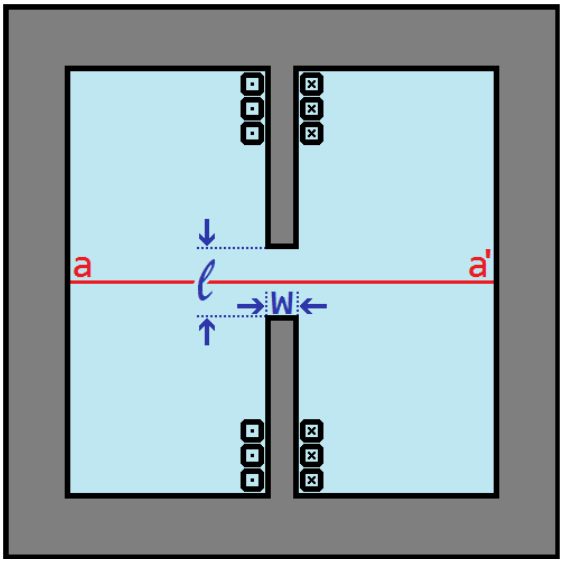

(b)

Figure 6: (a) machine producing flux perpendicular to patient, (b) 2-D drawing of machine. Focussing is desired along the line a-a' (not a physical part of the structure).

The field is generated using at least one pair of coils (i.e. one coil on either side of the body) to achieve the required flux penetration. The return paths of the flux are controlled using a material with a high magnetic permeability relative to the surrounding air. The return paths form a closed loop that makes up the frame of the machine. The machine is therefore symmetrical about the main coils. This choice of machine geometry allows for the addition of elements to either side of the coils, in order to achieve focussing whilst maintaining symmetry of the produced field pattern. A simple device, made to these specifications is shown in Figure 6. It can be seen that the device resembles a magnetic E-E core with an air gap introduced to the central leg (hereafter referred to as pole) of the E sections. The purpose of the air gap is to accommodate the thorax of the patient and therefore, it should be sufficiently large to do so. An air gap-length (l) of 40 cm is assumed to be sufficient. The centre poles, around which the main coils are placed (as seen in Figure 6b), are hereafter referred to as the main poles.

This section will attempt to analyse the results obtained when simulating the machine explained above without any additional attempts to focus the magnetic field. The goal of the focussing will then be to improve upon these results. The performance of this device for various air gap-lengths (l, Figure 6b) and pole-widths (w, Figure 6b) is now investigated.

A model of the machine was created using the finite element analysis (FEA) software, FEMM. By parameterising the model of the device and varying values, results are obtained for the relative magnetic field intensities for each configuration. Intuitively, the smaller the gap-length (*l*, Figure 6b) and wider the poles (w, Figure 6b), the less the influence of fringing flux. Therefore, it makes sense that when the gap-length is small relative to the pole-width ($l << w$), very little fringing flux is present and the field is approximately uniform in-between the top and bottom pole-faces. It makes sense to lump the pole-width and gap-length parameters into a single variable, since they both have an effect on the fringing flux. Simulations were run and the gap-length parameter was varied. This effectively varies the ratio: gap-length / pole-width (i.e. *l*/w).

These results are normalised to allow for easy comparison with each other and with results obtained later on. They are therefore described in terms of percentage of the maximum field strength for each simulation (along the line a-a' shown in Figure 6b, hereafter referred to as the measurement line). These results can be seen in Figure 7. The length of the air gap (*l*) and the width of the poles (w) have been reduced into a single variable by dividing the air-gap-length by the pole-width. This has been found to produce meaningful results due to the linear scalability of the machine, which will be explained later in this chapter. It must be noted that the measurement line is of constant length and is wider than the pole-width to include fringing flux. At low values of gap-length/pole-width, there is very little fringing as expected.

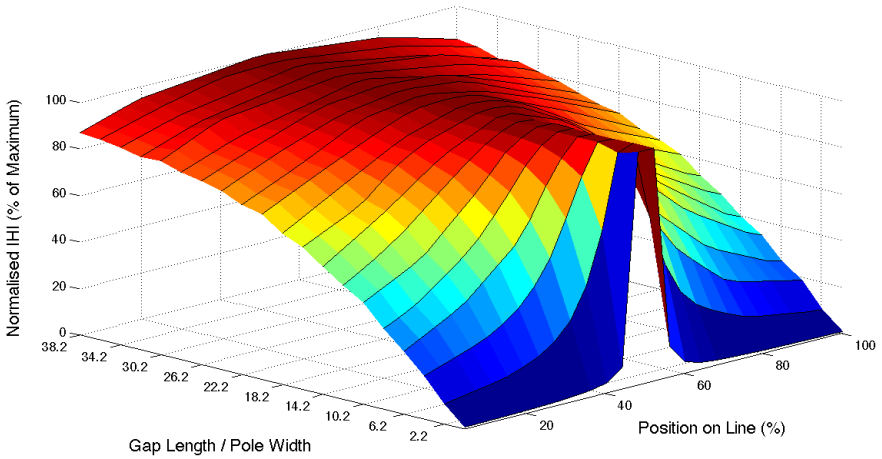

(a)

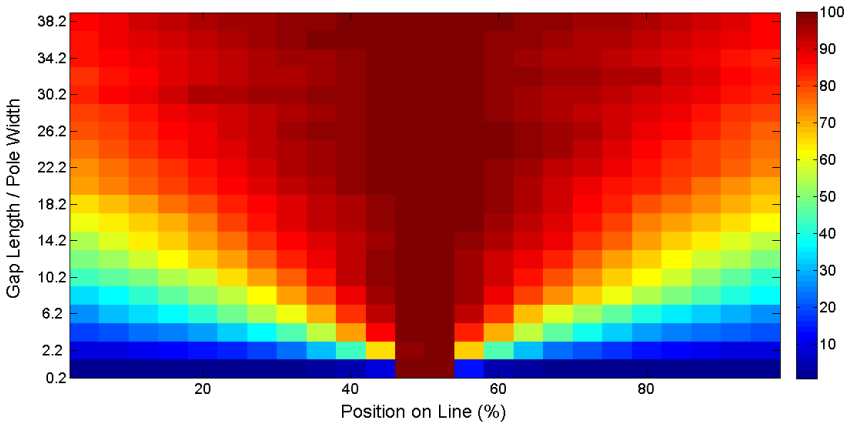

(b)

Figure 7: Magnetic field amplitude for different ratios of gap-length to pole-width. Measurements are taken on the line a-a' (Figure 6b) at arbitrary, equally spaced points.

From Figure 7, it can be seen that for small air gaps (where gap-length is smaller than pole-width), the field intensity decreases sharply when not directly in-between the poles. However, as the air gap increases in size, the flux lines tend to spread out as expected. In order to focus the field at the centre, it will be necessary to counteract the spreading of the flux lines. This is further demonstrated by Figure 8a, which shows the flux lines produced by two bar magnets aligned such that the magnets attract each other. Because the gap distance is significantly large, the flux lines between the poles are not well contained in the green area of the image. By creating flux lines in the opposite direction, in the same positions as the flux lines above and below the green area of the figure, a focussing effect can be achieved. This chapter will demonstrate the method by which this is performed. The desired ideal, focussed flux lines are shown in Figure 8b, in which the flux density is greatest at the centre of the green rectangle.

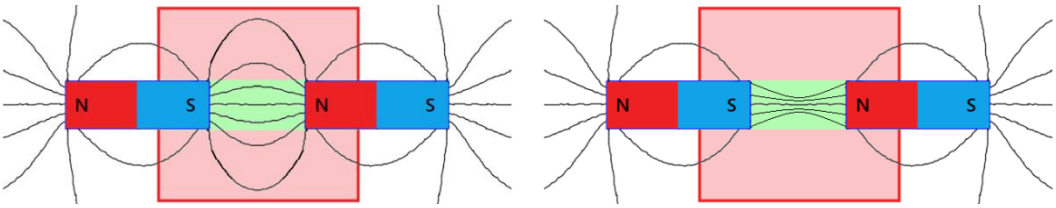

(a) (b)

Figure 8: (a) Flux lines occurring when two bar magnets are aligned such that they attract one another. The flux lines directly above and below the green rectangle are examples of flux fringing. (b) Example of flux lines occurring in an ideally focussed manner. The flux lines remain in the green rectangle and the flux density is highest at the centre.

3.3. PROOF OF CONCEPT

In order to demonstrate that magnetic field focussing is indeed possible, a simple simulation was performed. The configuration shown in Figure 6 was created in FEMM. Floating coils were then placed along the measurement line, on either side of the poles, as shown in Figure 9. These coils (hereafter referred to as the focus coils) carry current in the same direction as the main pole coils (hereafter referred to as the primary coils). The return flux lines from the focus coils oppose the flux generated by the primary coils. Vector summation occurs where the magnetic flux lines overlap. Some of the fringing flux is counteracted by the return flux from the focus coils, thereby increasing the magnitude of the gradient of the flux density pattern between the coils. It has therefore been shown that this configuration is able to produce the focussed magnetic field. The distance between the focus coils is varied and the effect on the output, as measured along the measurement line, is recorded. Figure 10 shows a series of results obtained with this approach.

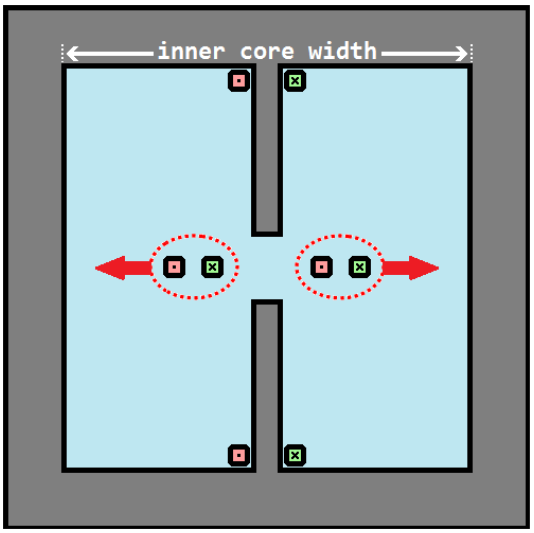

Figure 9: Machine with focus coils in the vertical centre, on either side of the main poles. Focus coils produce flux in the same direction as flux from main poles.

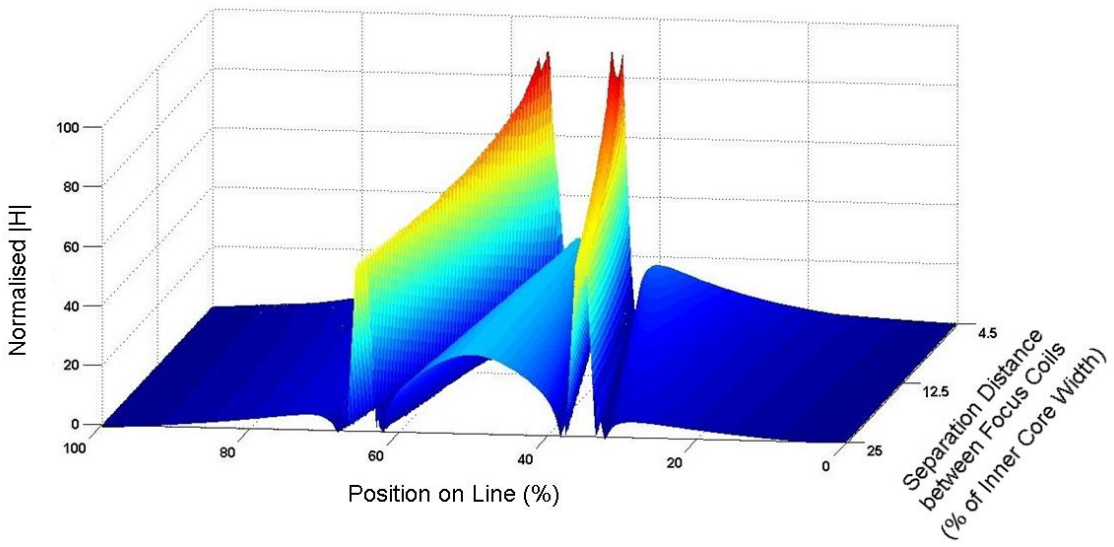

(a)

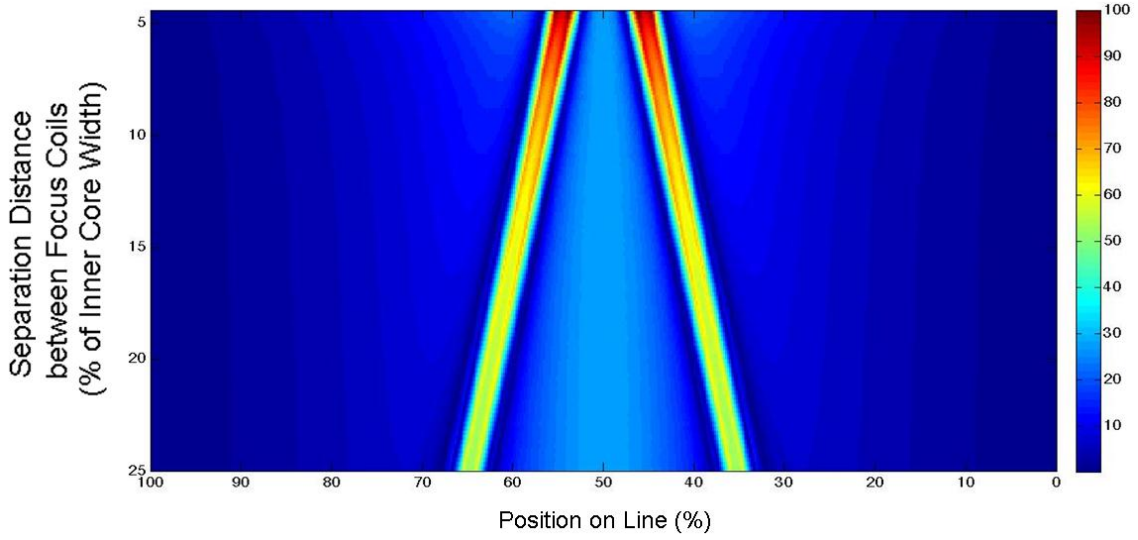

(b)

Figure 10: Simulation results showing proof-of-concept. The focussing improves as the focus coils are moved closer together.

Figure 10 shows the narrowing of the main, central peak as the focus coils are brought closer together. This result demonstrates that the focussing of a magnetic field, within near field distances, is indeed viable. It is important not to make direct comparisons between the result shown in Figure 10 and the results shown in Figure 7, since arbitrary values for pole-width (w) and gap-length (*l*) were chosen to obtain the results shown in Figure 10. A conclusion that can be drawn when comparing these two figures is that despite a high value for gap-length / pole-width (i.e. *l*/w) in the setup shown in Figure 9, the central peak remains far better defined than the peak shown in Figure 7 for similar *l*/w values.

The approach discussed here works best when the coils can be brought close together. However, sufficient space must exist between the focus coils to accommodate the patient. The effect created by bringing the focus coils close together cannot be reproduced by using focus coils placed further apart but with a larger MMF. From Figure 10, it can be seen that the central peak (i.e. the field due to the main coils) is focussed by the large spikes caused by the outer edges of the focus coils. The large spikes occur because the magnetic field intensity is high within the focus coils and the measurement line passes directly through the centre of the focus coils. Whilst changing the MMF of the focus coils does have an effect on the focussing, the most influential and immediate change is noticed by varying the spatial separation of the focus coils. It can be seen that this approach successfully improves the focussing of the field. Alternative methods for the production of the cancelling flux lines are therefore explored.

3.4. THE IDEAL CASE

The ideal, focussed case can be modelled as shown in Figure 11. Consider a core made from a material of infinite permeability. A section of the core gap contains air (shown in blue, Figure 11). The rest of the environment is made up of a theoretical material with a relative permeability of zero. If the centre legs of this machine are energised, the flux in the machine will be equal to the flux in the narrow channel of air, since the zero permeability material will not allow for any fringing to occur.

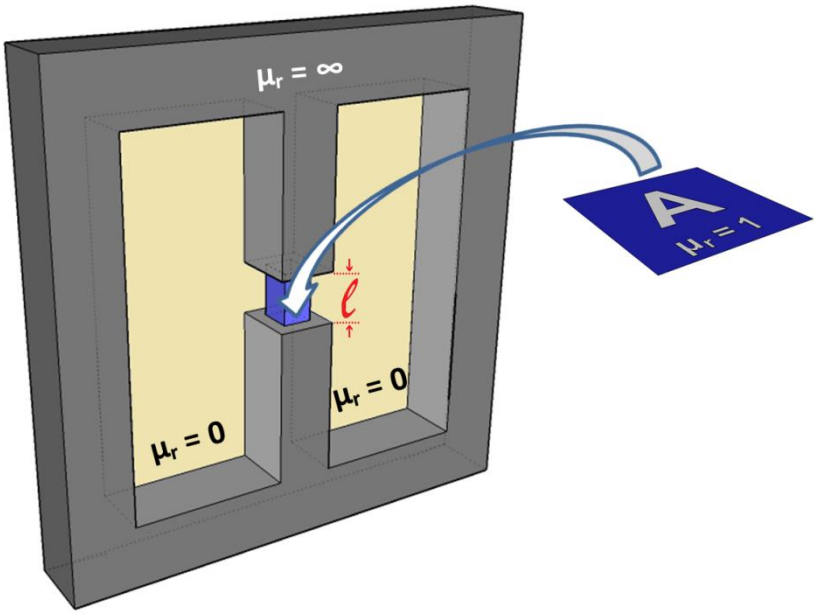

Figure 11: Configuration used to obtain an understanding of influential parameters and limitations of the focussing objective.

It is not possible to build the machine according to Figure 11, since the materials are only theoretical. It is however useful to imagine the focus poles as the equipment necessary to lower the effective relative permeability of the areas in which fringing flux is undesired.

Since the area of the air, A, in Figure 11 is known it becomes trivial to calculate the flux density that can be achieved in that channel and its relationship to the channel width and length. This is useful in order to understand the theoretical factors that play a role in focussing a magnetic field.

The air gap reluctance is dependent on its length and cross sectional area, as shown in equation 3.1.

$$\Re = \frac{\ell}{\mu A} \qquad (3.1)$$

The flux in the system will therefore be described by equation 3.2:

$$\Phi = \frac{Ni}{\Re}$$

$$= \frac{Ni\mu_0 A}{\ell} \qquad (3.2)$$

The flux density then becomes:

$$B = \frac{\Phi}{A}$$

$$= \frac{Ni\mu_0}{\ell} \qquad (3.3)$$

This is a well-accepted formula for the calculation of the flux density in free-space. However, it does manage to shed some light on the objective. There is no maximum to the focussing of the field and of all the properties of the air gap, only its length (*l*) affects the flux density that can be achieved. (The ideal core material will never saturate)

The important knowledge that can be obtained from this thought experiment is that the maximum flux density that can be achieved using a predefined MMF is inversely proportional to the gap-length. The focussing is indeed possible and alone imposes no theoretical flux density limit. As the gap-length is increased, a decrease in flux density will occur. This is due to the increased reluctance of the air gap.

3.5. DETAILED DESIGN

A closed solution for the optimal design of the complicated focussing device would be impractical to attempt due to the large number of variable parameters. Instead, FEA software was used to simulate variations of different parameters of a model. Analysis of the data arising from these simulations produced patterns from which a design technique could be formulated. Simulations of various scenarios were performed in order to best observe these patterns emerging. The model was created using practical constraints, governed by limitations and restrictions imposed by the dimensions of a human body. Specifically, the air gap that dominates the system design should be large enough to accommodate the thorax of a human adult. This constraint is further discussed later.

3.5.1. Approach

The design procedure will aim to maximise the focussing effect. It has already been shown that placing focus coils in the model, as shown in Figure 9, achieves a focussing along the measurement line. It is also clear that bringing the focus coils closer together can increase the focussing effect. However, this configuration has a major downfall. The coils need to occupy space that is reserved for the patient.

The focus coils are effective because their return flux is opposite in sign to the flux linking the top and bottom main poles. Fringing flux from the main poles is therefore largely cancelled out by the return flux of the focus coils. This is demonstrated by the configuration shown in the left hand side of Figure 12. In order to replicate this effect, without taking up physical space reserved for the patient, the focus coils are replaced by focus poles i.e. additional poles are added to the model on either side of both the top and bottom main poles. The flux produced by the focus poles must therefore share the same sign as the return flux of the original focus coils, as shown by the right hand side configuration in Figure 12. Similarly, further focussing may be achieved by attaching additional focus pole sets to the model. Each set of focus poles should emit flux that counteracts the fringing of the pole on its innermost side. The innermost focus poles should have an MMF that is opposite in sign to the MMF of the main poles. The next set of focus poles should have an MMF equal in sign to that of the main poles, etc. This type of setup has the added benefit of reducing the net flux in the return path of the machine (the frame), thereby reducing losses in those sections of the machine. The alternating of the MMF direction is shown in Figure 13. The four focus poles that directly neighbour the main poles will be referred to as the first set of focus poles or FP_1. If four more poles are added, they are referred to as FP_2 etc.

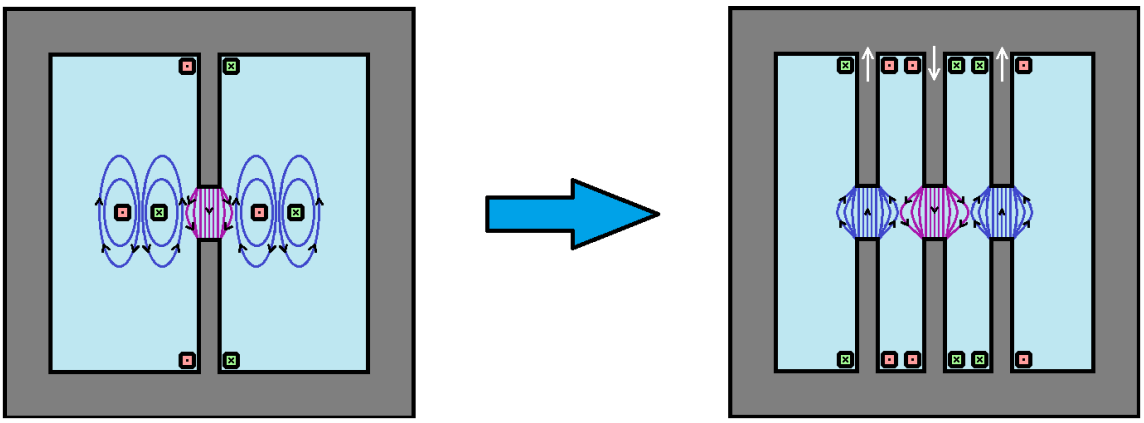

Figure 12: Focus poles replace focus coils in an attempt to achieve desired focussing whilst maintaining space for patient.

3.5.2. Resulting Complications

3.5.2.1. Unwanted Flux Loops

When the focus poles are included as described in section 3.5.1, flux between the oppositely magnetised poles creates a near uniform magnetic field in-between these poles, since the length of the poles is greater than the separation distance between them. The blue lines in Figure 13 show the flux lines that arise from this configuration. The magnetic field intensities between the pole-sides reach amplitudes in excess of that at the pole faces, since the separation between the poles (a, Figure 13), hereafter referred to as the pole-to-pole separation distance, is generally smaller than the patient-gap-length (*l*, Figure 6b). As a result, when the field amplitude in the patient is increased to high levels, the flux density in the poles will cause them to saturate, thereby increasing the effective patient-gap distance, since the permeability of the core material resembles that of air under saturation conditions [5]. As can be expected, with a larger gap-length (*l*), the focussing of the field is significantly reduced i.e. the fringing becomes more pronounced. It is therefore important that flux leaving and/or entering the sides of the poles is significantly reduced.

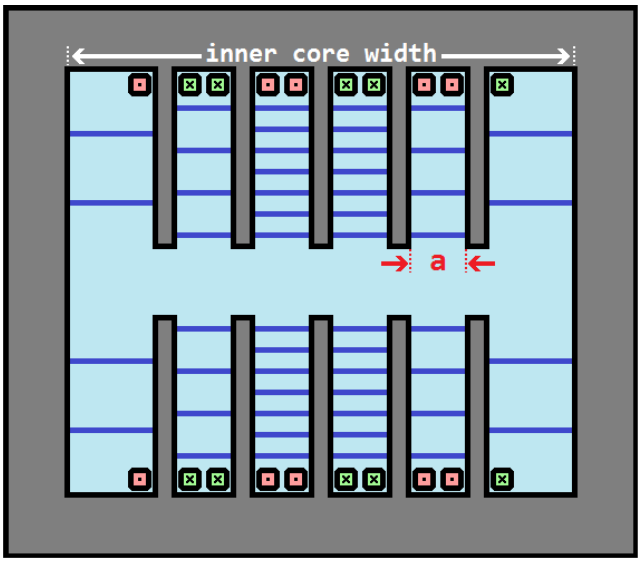

Figure 13: Machine with two sets of focus poles. Blue lines represent flux leaving and/or entering sides of focus poles. Required, alternating coil polarity is also shown.

In order to achieve this, it is necessary to block the flux from leaving and/or entering the sides of the poles. This is not a trivial task. Under DC conditions such as those in the magnetostatic FEA simulations, a material was placed between the poles. The material was assigned a relative magnetic permeability of approximately zero in order to block any flux from passing through it. This material was used throughout the design stage and allowed for the design to be performed under DC conditions. The only real material able to replicate this flux-blocking property is a superconductor. The ability of a superconductor to block flux has been described in chapter 2 of this dissertation. This material was useful in modelling the ideal case in which flux between the sides of the poles was completely eliminated. Its use therefore served as the ideal case. Similarly, the magnetic material used for the core was one of an extremely high magnetic permeability. It was decided to build the prototype using readily available materials at room temperature. It therefore became necessary to find an alternative solution to blocking the flux from entering/leaving the side of the poles. This was achieved by using eddy currents induced in copper "shields" to block flux penetration as per Lenz's law. This is further discussed in section 3.9 of this chapter.

3.5.2.2. Additional Areas of High Field Amplitude

The method by which the focussing effect is achieved creates additional magnetic field peaks and troughs, along the measurement line in the centre of the machine. Each additional set of poles will create an additional peak. This is shown in Figure 14. It quickly becomes evident that the more significant these focussing peaks are, the greater the focussing effect becomes. However, it becomes important to realise that the focussing peaks should not cause the magnetic field within healthy cells to be above the previously defined safety limit i.e. the peaks caused by the focus poles should not be sufficient in magnitude to cause thermal damage of healthy cells.

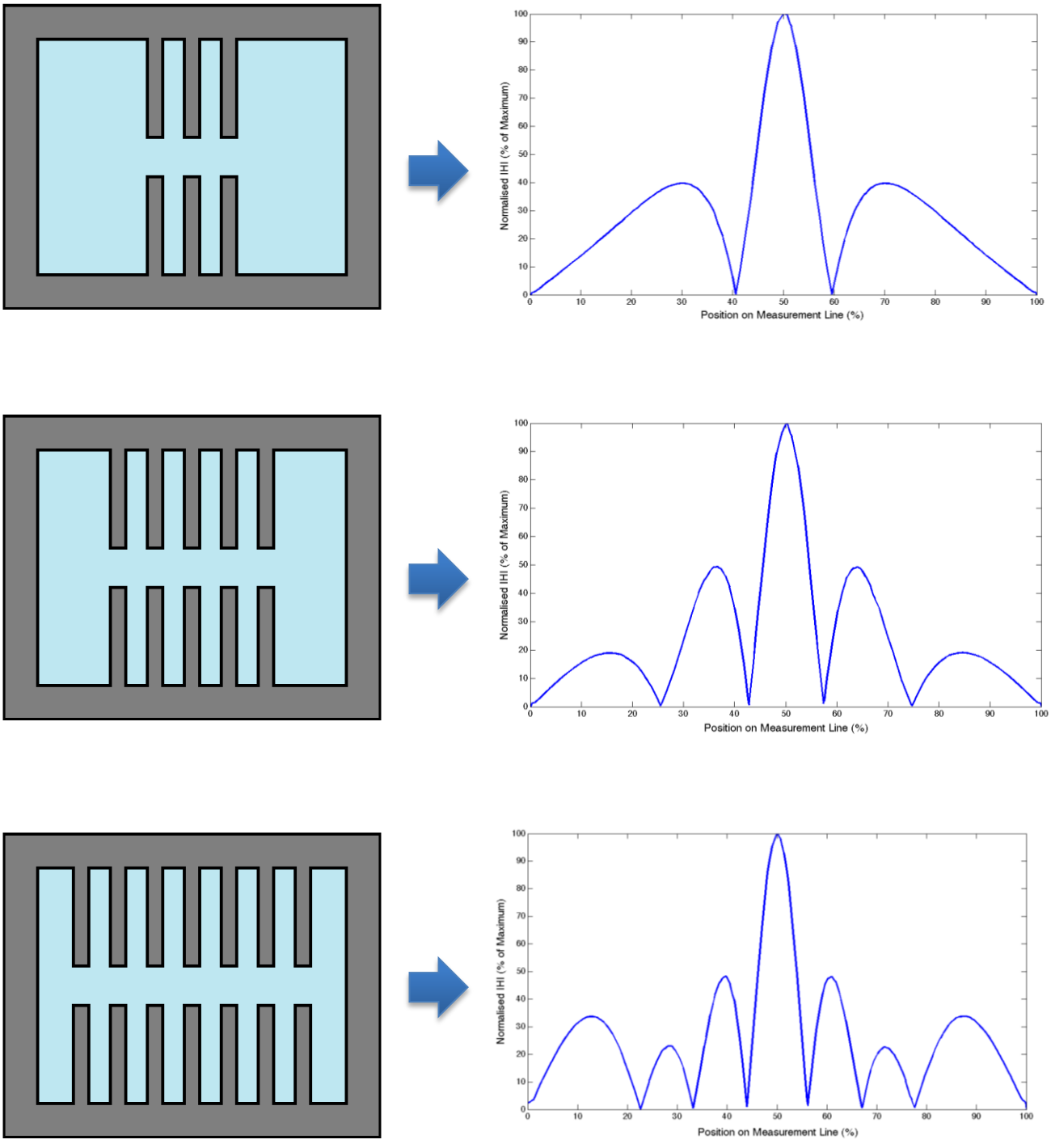

Figure 14: Peaks of field amplitude, along the measurement line, resulting from the addition of focus poles.

In order to proceed with the design, some constraints were placed on the magnitude of the peaks caused by the focus poles. Any solution that resulted in focussing peaks greater in amplitude than 50% of the primary peak would be discarded. This ensures that the only the central peak is sufficiently strong to provide therapeutic benefit, whilst the other peaks remain too low to cause unacceptable levels of damage.

3.5.3. The Model

Boundary conditions were placed on the physical dimensions of the machine. These boundary conditions were chosen based on practical considerations. The model was proportioned such that the air gap was large enough to fit the torso of an average human adult. For this, 40 cm was deemed to be sufficient. A circle of radius 40 cm, in the centre of the machine, was therefore reserved for the patient and no machine or focussing equipment was allowed to occupy the space within the circle. A maximum machine size of 2m by 2m was used in the design. This was deemed to be large enough to accommodate the focus poles, coils and patient. All dimensions are scaled as described in the following section. However, the patient gap distance (*l*) as a percentage of the inner core width (Figure 13) always remains constant.

3.5.4. Scalability

Although the machine requires certain dimensions as discussed in section 3.5.3, the entire geometry and its output can be scaled proportionally. That is: by multiplying every dimension as well as the MMFs of each coil by a constant factor *k*, the output flux amplitude remains the same when plotted against distance (as a percentage of the inner core width). This is due to the fact that when all dimensions are scaled by *k*, the change in flux as a result of the change in reluctance is counteracted by the change in cross sectional area. This effect causes equations 3.3 and 3.4 to be equal, as shown below.

Original configuration: $B = \frac{(Ni) \times \mu}{l}$ (from 3.3)

Scaled configuration: $\Re = \frac{k\ell}{\mu k^2 A} = \frac{1}{k} \times \frac{\ell}{\mu A}$

$$B = \frac{\phi}{k^2 A} = \frac{Ni}{\Re k^2 A} = \frac{(Nik) \times k\mu A}{lk^2 A}$$

$$= \frac{(Ni) \times \mu}{l} \quad (3.4)$$

Similarly, the field amplitude values are linearly related to the MMF in the coils since changing the MMF by a constant factor will change the flux produced by that same factor - provided the reluctance remains fixed. The focussing of the field along the measurement line shown in Figure 6b can therefore be compared to the focussing along the same line using a different configuration. This first requires normalisation of the results, which is achieved by representing all values as percentages of the maximum value, occurring at the centre of the measurement line. This is valid because it is the focussing that is being compared i.e. the gradient of central peak of the field amplitude pattern. The relative MMF to produce that pattern is not relevant to the optimisation, since it will be made whatever it needs to be to achieve the required focussing.

3.5.5. Variable Parameters

The proposed design results in a complex geometry. The configuration can be optimised by varying individual gap-lengths, individual pole-widths or individual MMFs. It is evident that there are many different parameters that can be varied in order to achieve a change in the focussing of the magnetic field. With the addition of more focus poles, the number of total solutions increases exponentially. Another parameter that is introduced when focus poles are added is the distance between the new focus pole and the pole on its innermost side i.e. the pole-to-pole separation distance. It quickly becomes apparent that an exhaustive search is not practical when so many variables exist. This section aims to demonstrate that by choosing to vary certain parameters, other values can be fixed and an optimum result can still be achieved. This greatly reduces the complexity of the brute force optimisation approach, since fewer variables exist.

In order to demonstrate the feasibility of this approach, it becomes necessary to show that the same results can be obtained by using different parameters as the optimisation variables. This will be revealed by setting one quantity as constant and varying another and then swapping the constant and variable quantities. If the outputs produced are identical, then the properties are interchangeable in the optimisation process and it becomes a choice as to which to vary. This can be understood intuitively. If it is the fringing flux of the focus poles that is responsible for the focussing effect, then the fringing flux must reach some optimal value to achieve a desired result. There are several ways to influence the fringing flux i.e. change the gap-length to pole-width ratio (l/w) or change the MMF applied to the focus poles. Therefore, the fringing flux will be affected by varying either the pole-widths (w), focus pole gap-lengths or the applied MMF. Furthermore, it should not be

necessary to vary all of the above mentioned parameters since any combination of the three should be possible to replicate by fixing two and varying the third.

Table 1 and Figure 15 show different configurations that produce outputs of high similarity. The output in this case is the magnitude of field intensity along the measurement line (line a-a', Figure 6b). The outputs are shown in Figure 16. The resultant field patterns differ slightly due to the discrete steps used by the optimisation procedure i.e. the variable was modified by a constant amount until a similar output was produced. The field patterns produced by values in-between the steps are unknown and may closer resemble the outputs of the other scenarios.

Table 1: Three scenarios in which different parameters are varied to produce the same output. The blue blocks with the bold text mark the parameter that was varied in each scenario. It can be seen that only four of the six parameters are the same for any two scenarios.

	Scenario 1	Scenario 2	Scenario 3
Gap length (*l*)	**48 cm**	40 cm	40 cm
Main pole MMF	1 A.t	1 A.t	1 A.t
Focus pole MMF	0.5 A.t	**0.2865 A.t**	0.5 A.t
Main pole width (w)	10 cm	10 cm	10 cm
Focus pole width	10 cm	10 cm	**1 cm**
Pole-to-pole separation distance	1 cm	1 cm	1 cm

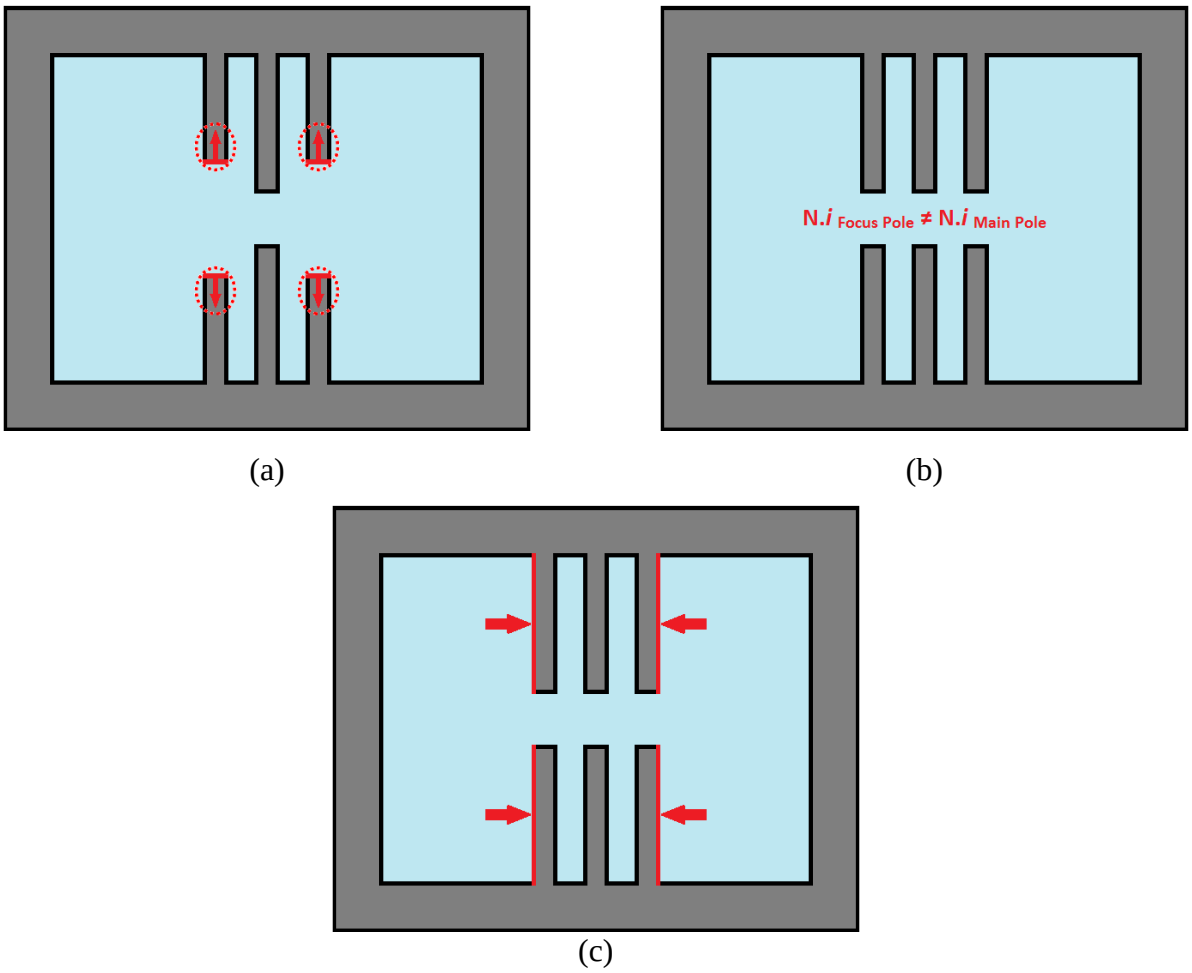

Figure 15: Illustrations of (a) scenario 1, (b) scenario 2 and (c) scenario 3. All illustrations show the adjustable parameter as can be seen in Table 1.

By decreasing the width of the focus poles whilst maintaining a constant gap-length, greater fringing occurs of the flux set-up by the focus poles. This option results in improved focussing since this fringing is responsible for counteracting the fringing of the primary field. However, changing the MMF of the focus poles or keeping the focus poles widths constant and increasing their gap-lengths can replicate the result. This property has been verified using finite element simulations. The simulations were performed using one set of focus poles as this was the simplest configuration. Each scenario required two quantities to be uncommon to the other scenarios i.e. out of the six properties shown in Table 1, only four are common between any two scenarios. One of the remaining quantities was the variable. The other quantity forced the optimisation procedure to produce a unique machine configuration. If the second quantity was not made different, then the simulation would alter the variables until all parameters in the machines were identical. Figure 16 shows that the three scenarios produce can produce similar results.

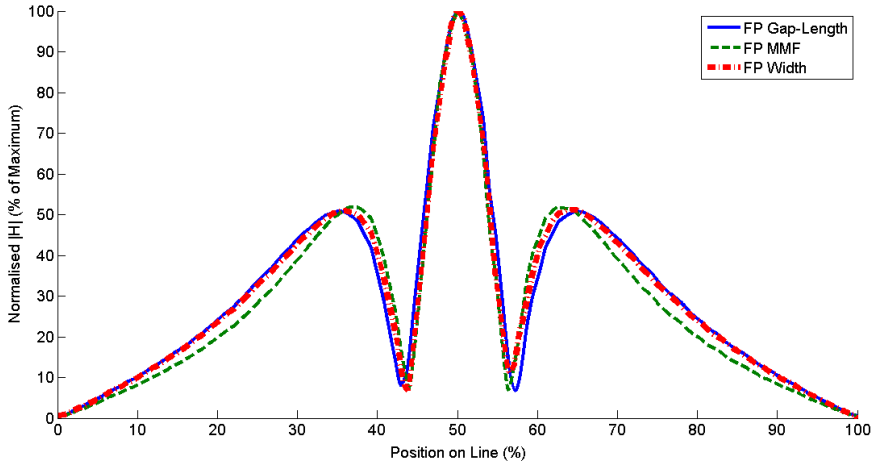

Figure 16: Outputs of simulation showing very similar results produced by varying different parameters in each case.

3.5.6. Further Design Decisions

3.5.6.1. Fringing Distance

The ultimate goal of this research is to create a magnetic field peak in the centre of the machine, with the highest possible levels of attenuation on either side of that peak. The higher the attenuation of the magnetic field, the more focussed it is. In order to easily quantify and compare the outputs from the different configurations simulated, the average tangent was considered. This value was obtained by examining how much distance it takes along the measurement line, from the machine centre, to attenuate from the maximum magnetic field value to the point at which the central peak has attenuated by 50%. Since the outputs from the various configurations have been normalised and converted to percentages, the numerator of the tangent equation will always be 50% (or half of the normalised, maximum value). It therefore becomes more useful to use only the distance necessary for the focussed field to attenuate to 50% of its value. This will be referred to as fringing distance (FD) for the remainder of this dissertation. This is shown in Figure 17.

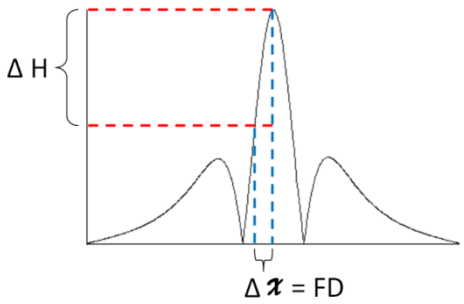

Figure 17: Explanation of fringing distance (FD). Δx is the change in distance along the measurement line.

3.5.6.2. H_{pole}:H_{centre}

An otherwise important concern and a secondary design goal, is to achieve a suitable H_{pole}:H_{centre} ratio. This is the ratio between the field amplitude at the main pole-face to the field amplitude at the centre of the machine, as shown in Figure 18. Up until now, only the magnetic field along the measurement line has been discussed. Therefore focussing has been performed in one plane only. The field amplitude at the main pole-face is larger than the amplitude at the centre of the machine. This results in the occurrence of high field amplitudes within healthy cells above and below the tumour. It is therefore desirable to minimise the H_{pole}:H_{centre} ratio. A high ratio can be dealt with by continuously rotating the machine relative to the patient so that heating of the healthy cells is minimised everywhere besides for the target region at the machine's centre.

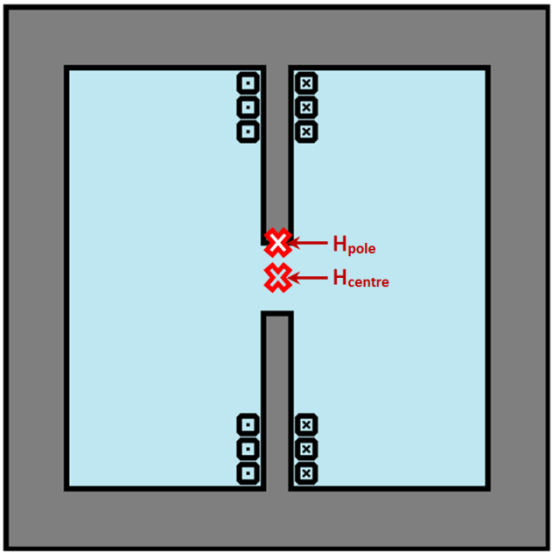

Figure 18: Positions of H_{pole} and H_{centre}.

3.5.6.3. Additional Constraints

In order to proceed with the design, it became necessary to constrain some additional parameters. The widths of the focus poles are equal to the width of the main pole (w, Figure 6). Additionally, all pole-to-pole separation distances are equal to each other and to the width of the poles (w, Figure 6). This separation distance is always assumed to be large enough to accommodate the required number of turns of the conductor used to produce the MMF. An additional concern is to allow enough room for a shield of sufficient thickness to effectively block the flux from leaving or entering the sides of the poles (as discussed later). Two different designs were investigated. In the first configuration, the

gap-lengths of the focus poles are fixed and the MMF of each focus pole is varied. In the second configuration, the MMFs are equal and fixed for all poles and the focus pole gap-lengths are varied.

3.5.7. Analysis of Simulation Results

The analysis of this data was performed using the following algorithm. A limit was imposed on the amplitude of the field strengths of the side lobes. An arbitrary value was chosen which limited the field amplitude of any side lobe to 50% of the field amplitude of the primary, central lobe of the magnetic field along the measurement line. It was then decided that the desired focussing could be quantified by determining the distance over which the primary, central lobe attenuated to 50% of its original value in terms of field strength. A smaller distance corresponds to greater focussing. The configuration that produced the smallest distance, between the machine centre and the position marking 50% of the central peak, was deemed to be the optimum configuration for that particular design. Any configuration producing side lobes (peaks) larger than 50% of the main lobe in terms of field intensity were immediately discarded. Additionally, any configuration that produced a pattern which did not attenuate to below 50% of the magnetic field intensity of the main lobe was also discarded. Figure 19 shows the process described above.

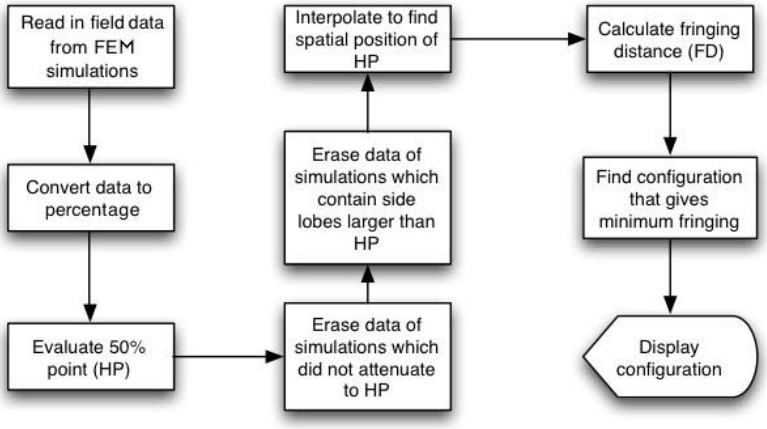

Figure 19: Algorithm used to analyse data obtained from FEMM package.

3.5.8. Magnitude of Magnetic Field Intensity at Machine Centre

The centre of the machine should coincide perfectly with the position of the tumour since, at the machine centre, the magnetic field intensity will exceed the safety limit for healthy cells. The actual value for the field intensity, H, will depend on the particular configuration of the machine (pole widths, MMFs and gap-lengths). It is difficult to predict the field intensity for any particular configuration without adding more variables to the design procedure, thereby greatly increasing the

complexity of the design. For this reason, the field intensity will not be considered for the remainder of this chapter. It is far more important to optimise the design by fringing distance and H_{pole}:H_{centre} ratio. After a suitable configuration is found in terms of those parameters, the required field intensity can be achieved by simply increasing all of the MMFs in the machine by the same factor. This remains true until the machine begins to saturate or when all of the poles have fully saturated. The saturation behaviour of the machine is described in section 3.8.

3.6. DESIGN RESULTS

All results were obtained using the FEMM finite element analysis software package. The quantity *fringing distance* (FD) is given in percentage of the inner core width of the machine so as to accommodate for the scalability of the system. *Fringing distance* is defined as the distance taken for the magnetic field along the measurement line to attenuate from its maximum to 50% of its maximum on the main peak. *Fringing distance* is also the quantity used to assess the effectiveness of the focussing and determine which configuration produces optimal focussing. Optimal focussing is the smallest fringing distance that occurred for a particular configuration. Similarly, the pole width axis of the graph has been represented as a percentage of the inner core width. Pole width is always used as a design parameter because different pole widths produce different outputs and require different configurations (MMFs or gap-lengths) in order to achieve optimal focussing.

Finally, as discussed in section 3.5.6.2, the quantity H_{pole}:H_{centre} Ratio describes the ratio of the magnetic field intensity at the pole face to the magnetic field intensity at the centre of the machine. If the machine is set to revolve around the patient to reduce the heating of healthy tissue, it becomes important to ensure that no part of the field that will revolve through the patient is significant in amplitude to cause eddy currents that would supply a dangerous level of nerve or muscle stimulation. The exact magnitude of field amplitude required to create this effect is dependent on the precise position in the body around which the machine is revolving since muscle stimulation in certain regions may be tolerated.

3.6.1. Optimisation using Relative MMFs

The MMFs of the focus poles were varied until the optimum focussing was achieved. The configuration used in this design process resembled that of Figure 15b. Optimising using MMF has several advantages. The machine is simple to build since all poles have the same dimensions. It is

also easier to adjust the current in the coils around the poles (thereby adjusting the MMF) than to adjust the gap-lengths making fine-tuning simpler and even creating the opportunity for machines that can be adjusted during operation. The disadvantages of this approach are that it requires more material (for both the poles and the shields) and it is less efficient. The loss of efficiency is due to the close proximity of the pole faces forming undesired flux paths. As a result, some of the flux circulates between neighbouring poles rather than passing through the space reserved for the patient. This is shown in Figure 20. When the gap length optimisation technique is used, the variations in the focussing poles' gap-lengths result in a larger distance between the pole faces of neighbouring poles. This results in more flux passing through the patient area.

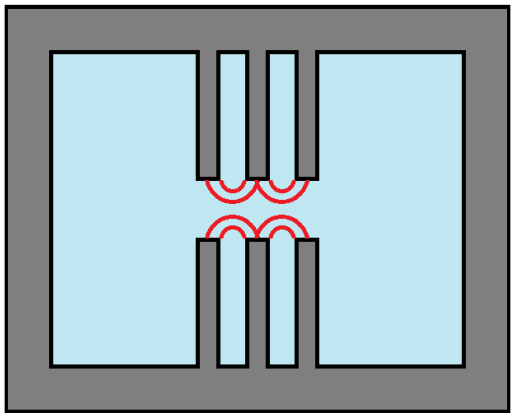

Figure 20: Flux lines (shown in red) circulating between neighbouring poles.

The investigation was repeated for one set, two sets and three sets of focus poles and various pole-widths and hence various pole-to-pole separation distances, since *w* (Figure 6b) has been set equal to *a* (Figure 13) as described in section 3.5.6.3. The results of the simulations for the two focus pole sets have been plotted against pole-width in Figure 21. All MMFs are shown as a percentage of the main pole MMF and widths are expressed as a percentage of inner core width.

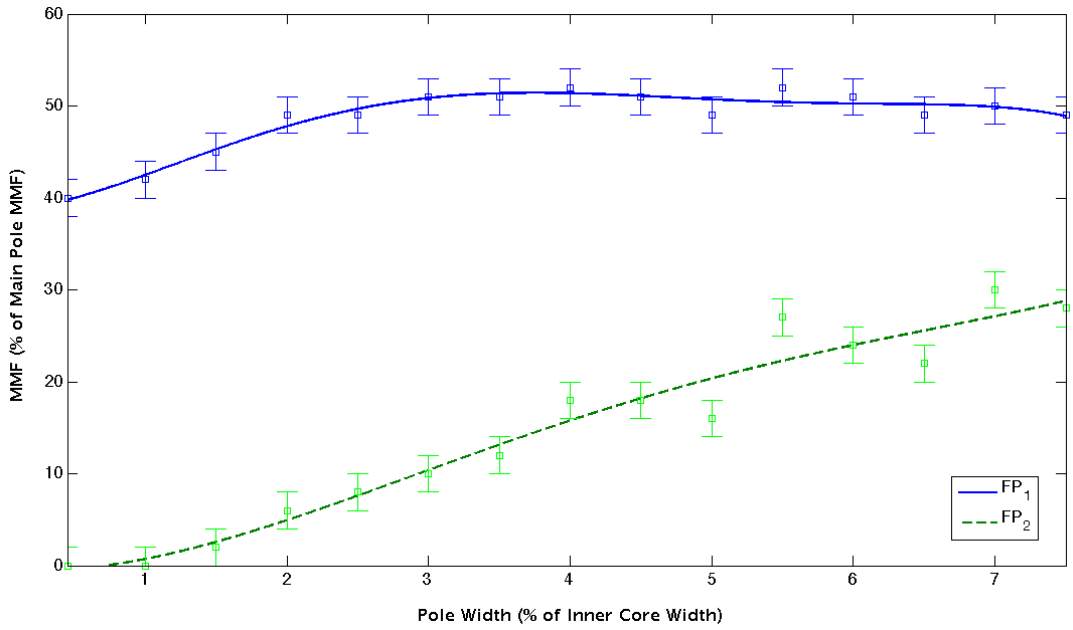

Figure 21: Relative MMFs of focus poles to achieve optimum focussing.

In Figure 21, a curve has been fitted to data points in an attempt to extract a trend. It is important to remember that a brute force optimisation procedure was used to obtain the values for the relative MMFs. This means that the MMF was increased by a fixed discrete amount with each iteration. Therefore, there is an MMF slightly larger or smaller than the one shown which would result in a slightly more focussed output. The discrete steps are taken into account by the error bars in the curves. The trend line should be allowed to differ from the obtained values by the fixed amount used in the iterative optimisation procedure. The trend lines, shown in Figure 21, were adjusted until this requirement was met.

3.6.2. Optimisation using Gap-Lengths

Focussing can be achieved by setting the MMFs of all poles to an equal, constant amount and varying the focus poles' gap-lengths. This configuration resembles that shown in Figure 15a. Optimising using gap-lengths has several advantages. The machine is more efficient in terms of flux density at the centre per A.t. at the poles. This is a result of the larger separation distances between neighbouring pole faces, presenting a larger reluctance to magnetic flux. This encourages the flux to pass through the patient region rather than looping back through a neighbouring pole. Additionally, less material is required. The disadvantages of this approach are that it is more difficult to build and to fine tune.

The gap-lengths of the focus poles were varied until the optimum focussing was achieved. As done in the MMF investigation, this procedure was repeated for one, two and three sets of focus poles and for various pole-widths. The configurations that achieved the best results for the two focus pole set model have been shown in Figure 22.

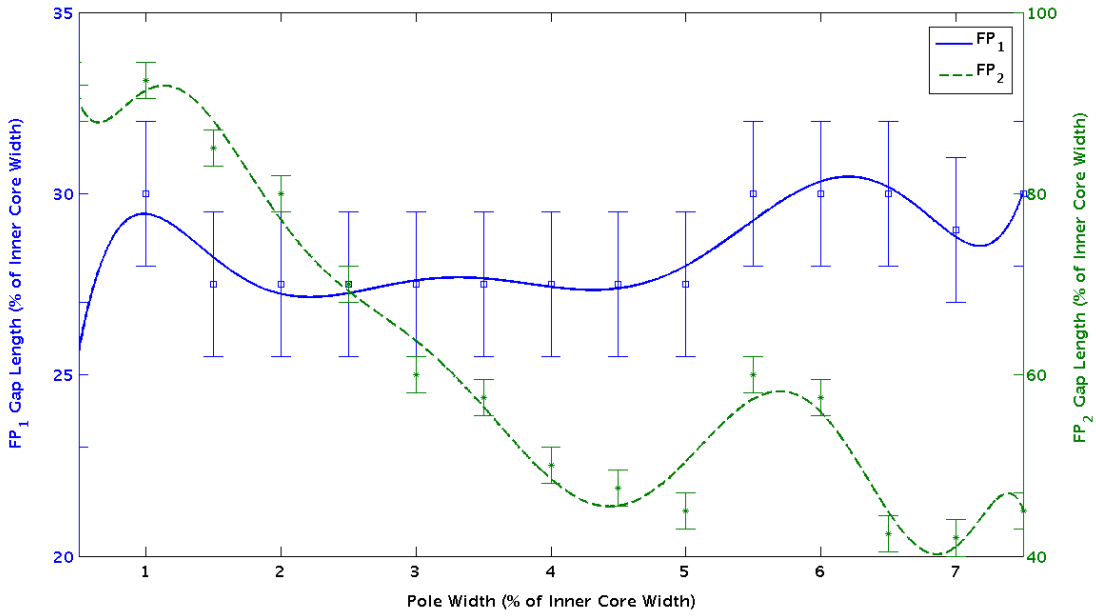

Figure 22: Relative focus pole gap-lengths to achieve optimum focussing

Once again a curve has been fitted to the data points in order to visualise a trend. The accuracy of the optimisation method used for the gap-length curves is also limited by the discrete, finite increments of the lengths applied with each iteration. By decreasing the size of the increments used in the simulations, a solution may be obtained that provides marginally improved performance. This would come at the expense of simulation time.

3.6.3. Output of the Optimisations

The shape of the magnetic field intensities, along the measurement line, that occur when the machine is setup according to Figure 21 or Figure 22 resemble the shape shown in the right hand side of the two focus pole diagram in Figure 14.

By numerically evaluating the fringing distance occurring when the machine is setup according to Figure 21 or Figure 22, it becomes possible to plot the fringing distance obtained for all the different pole-widths that were simulated. Similarly, the H_{pole}:H_{centre} ratio, obtained from each configuration, can be plotted against pole-width.

Figure 23 and Figure 24 provide the H_{pole}:H_{centre} ratio and the fringing distance versus pole-width for MMF optimised and gap-length optimised two focus pole sets models respectively.

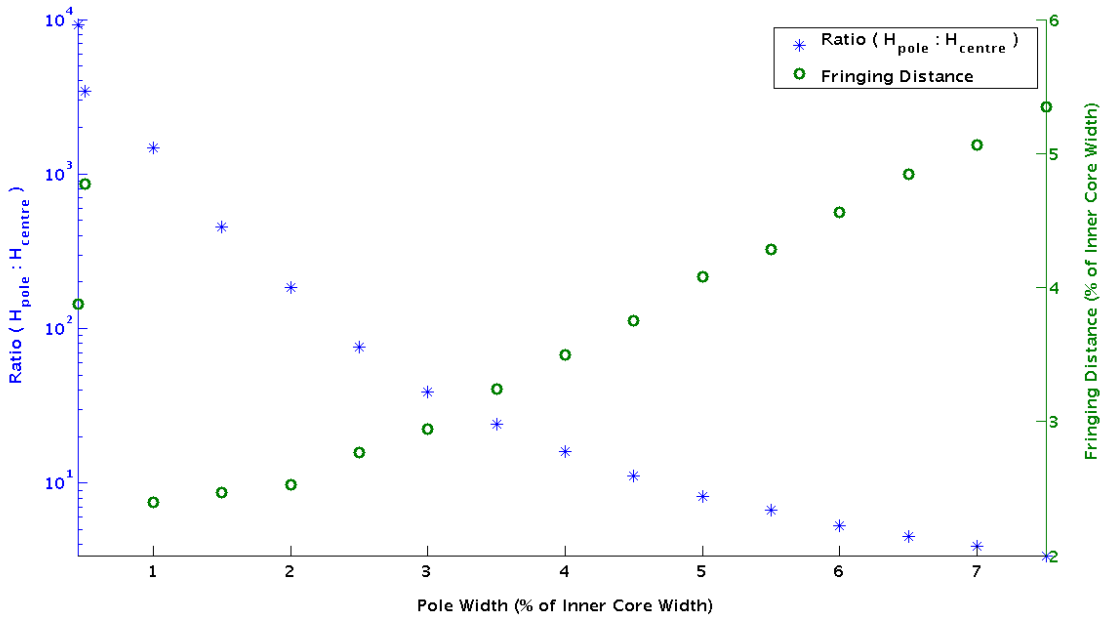

Figure 23: H_{pole}:H_{centre} Ratio and Fringing Distance obtained when MMFs applied to FP_1 and FP_2 are setup according to Figure 21.

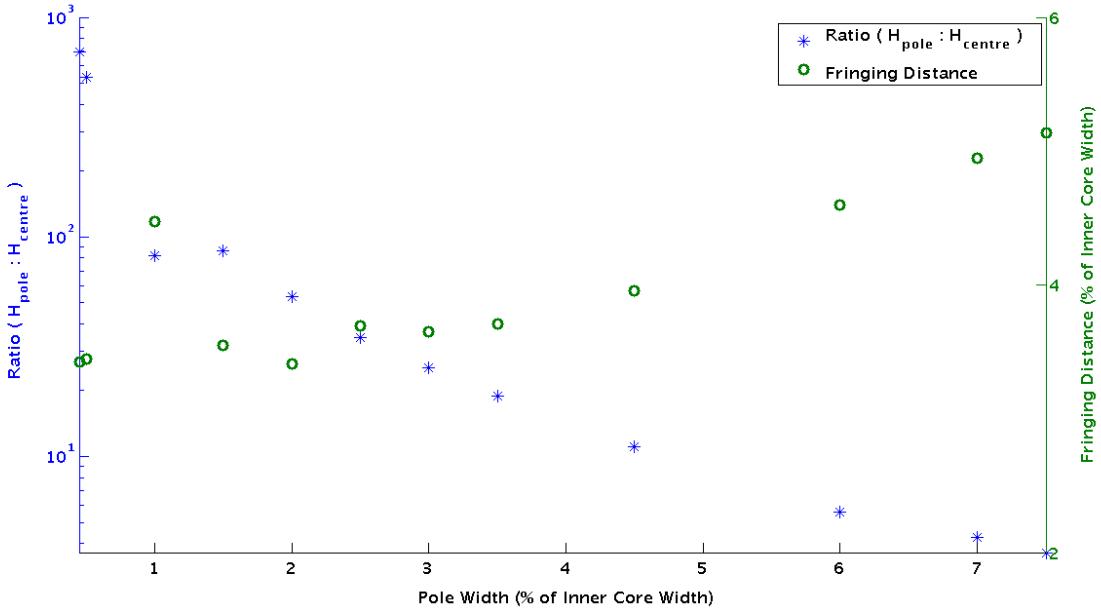

Figure 24: H_{pole}:H_{centre} Ratio and Fringing Distance obtained when gap-lengths of focus poles are setup according to Figure 22.

The above graphs demonstrate that a more focussed field often comes at the expense of a high H_{pole}:H_{centre} ratio. This means that at the design stage, a decision must be made regarding the maximum H_{pole}:H_{centre} ratio that can be tolerated. There is then a trade-off between the fringing distance (how well the machine will focus the field) and the H_{pole}:H_{centre} ratio.

3.6.4. Number of Focus Pole Sets

Simulations were performed and optimum parameters were obtained for one set, two sets and three sets of focus poles – for both MMF optimised and gap-length optimised configurations. The fringing distance and H_{pole}:H_{centre} ratio versus width graphs for one focus pole set and two focus pole sets have been combined in Figure 25. Similarly, Figure 26 shows the combined results for two focus pole sets and three focus pole sets. Both figures are for the MMF optimised system. Similar behaviour is exhibited by the gap-length optimised system.

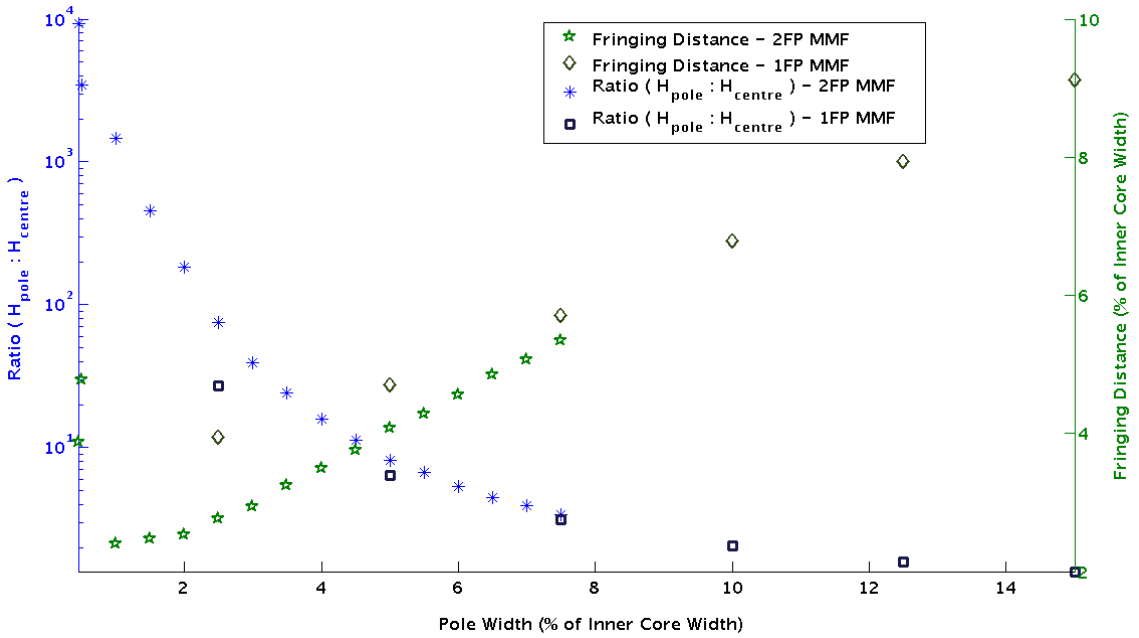

Figure 25: Comparison between outputs of two focus pole sets model and one focus pole set model (MMF optimised)

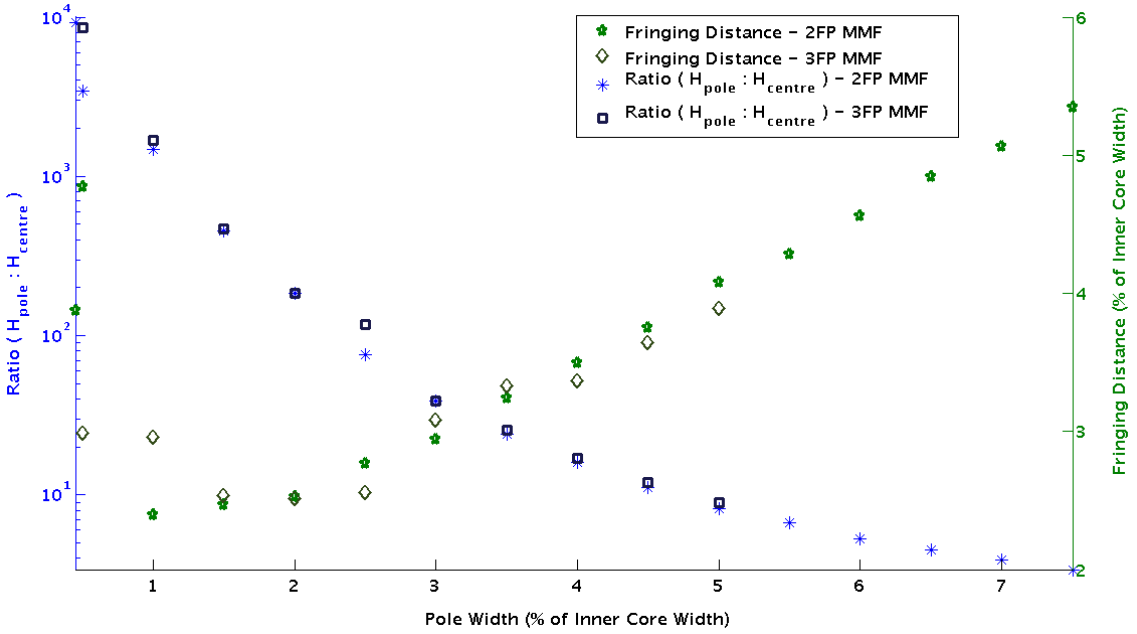

Figure 26: Comparison between outputs of two focus pole sets model and three focus pole sets model (MMF optimised)

Figure 25 and Figure 26 show that for a given pole-width, the H_{pole}:H_{centre} ratio remains fairly constant regardless of the number of focus poles in the system. A clear improvement in fringing distance can be seen in Figure 25, when changing from the one focus pole model to the two focus pole model. From Figure 26, the fringing distance of the two focus pole model and of the three focus pole model are very similar, indicating that there is very little benefit to be gained by using more than two focus pole sets.

The results presented in this section have been for the two focus pole model since its performance is significantly better than the one focus pole model and since very little benefit is gained when using the more complicated three focus pole model. The design curves for the one focus pole set and three focus pole sets can be found in appendix A.

3.7. DESIGN PROCEDURE

It becomes important to have a standardised method for designing the focussing device. As a result, the objective of this section is to demonstrate such a process, by which the entire design methodology has been simplified using graphs. The graphs aid in the design of any system that shares the constraints previously discussed. This also allows for machines that adjust themselves in real time to best treat a specific patient.

When analysing the trends in section 3.6, the first step was finding the optimum MMF or gap-length configurations for various pole-widths and then observing the outputs produced by each configuration. It is now possible to develop a design procedure for the machinery used to focus the magnetic field. In order to do this, the concepts discussed in section 3.6 must be approached in reverse order. Now that the data is available, it is possible to specify the H_{pole}:H_{centre} and fringing distance that is required for the specific patient.

Figure 23 or Figure 24 is then used to determine a pole-width that will satisfy both of these requirements. Once a pole-width is obtained, Figure 21 or Figure 22 can be used to determine the relative MMFs or gap-lengths required to achieve the desired focussing and H_{pole}:H_{centre} ratio.

The design procedure is more clearly explained using an example. Consider the system described below.

A two metre by two metre machine (inner core width) is required which produces a focussed magnetic field which attenuates from its maximum in the centre to 50% of the maximum in less than 10 cm. The H_{pole}:H_{centre} ratio is required to be less than 20:1. An MMF controlled system (equal gap lengths) is specified.

The proposed design procedure follows five steps:

1. Decide whether a gap-length controlled system or MMF controlled system is more appropriate/convenient.
2. Specify a maximum H_{pole}:H_{centre} ratio and a minimum fringing distance for the machine.
3. Using Figure 23 for an MMF controlled system or Figure 24 for a gap-length controlled system, find the pole-width that satisfies both the H_{pole}:H_{centre} requirement as well as the fringing distance requirement.
4. Using the pole-width determined in step 3, along with Figure 21 for an MMF controlled system or Figure 22 for a gap-length controlled system, read off the values of the MMF or gap-length for each focus pole.
5. Convert the pole-widths and MMFs or gap-lengths from percentages to real values and apply to machine design.

The five steps will now be applied to the system in the above-mentioned example. An MMF controlled system is specified so Figure 23 and Figure 21 will be used. A maximum H_{pole}:H_{centre} ratio of 20:1 and a fringing distance of 5% has been stipulated (10 cm of 2 m).

From Figure 23, it can be seen that at a pole-width of 4% of the inner core width, both the H_{pole}:H_{centre} ratio and the fringing distance requirements are met. A pole-width of 4% is then used for the width of all poles as well as the pole-to-pole separation distance.

Figure 21 is then used to determine the relative MMFs that must be applied to the focus poles in order to achieve the output described by Figure 23. Figure 21 shows that the inner set and outer set of focus poles must have an MMF of 52% and 18% of the main pole MMF respectively.

Finally, the percentages obtained should be converted to physical dimensions so that the machine can be built. A pole-width of 4% of the inner core width means that pole-widths (both main and focus poles) as well as the pole-to-pole separation distances should be 8 cm. Additionally, the MMFs applied to the inner set (FP_1) and outer set (FP_2) of focus poles should be 52% and 18% of the main pole MMF respectively. This can be achieved by either using less turns in the coils around the focus poles, less current through the coils or any combination that provides *N.i* values of 0.52 and 0.18 for FP1 and FP2 respectively (relative to the main pole MMF). This system would achieve a flux density, at its centre, of approximately 0.19 mT if the main pole MMF was 1 A.t.

3.8. SATURATION BEHAVIOUR

From Figure 21, it can be seen that the MMF applied to the main pole is always greater than the MMF applied to the focus poles in order to achieve the focussed effect. This means that the when a high output is required and the MMFs are increased, the sections of the machine with the highest flux density will be the main poles. Similarly, from Figure 22, it can be seen that the gap-length is always greater for the focus poles towards the ends of the machine than those towards the machine centre. A larger gap-length results in a larger reluctance in that flux path and therefore a lower flux. Once again, the sections of the machine with the highest flux density will be the main poles.

In both the MMF optimised system and the gap length optimised system, the second and third highest flux densities will occur in the first and second set of focus poles respectively. The frame of the machine (the return path) will have a low net magnetic flux density due to its large cross sectional area and the cancellation of the fluxes from the poles which are opposite in direction. This

is shown in Figure 27. This means that a relatively slim frame could be used without sacrificing performance, in order to save on materials.

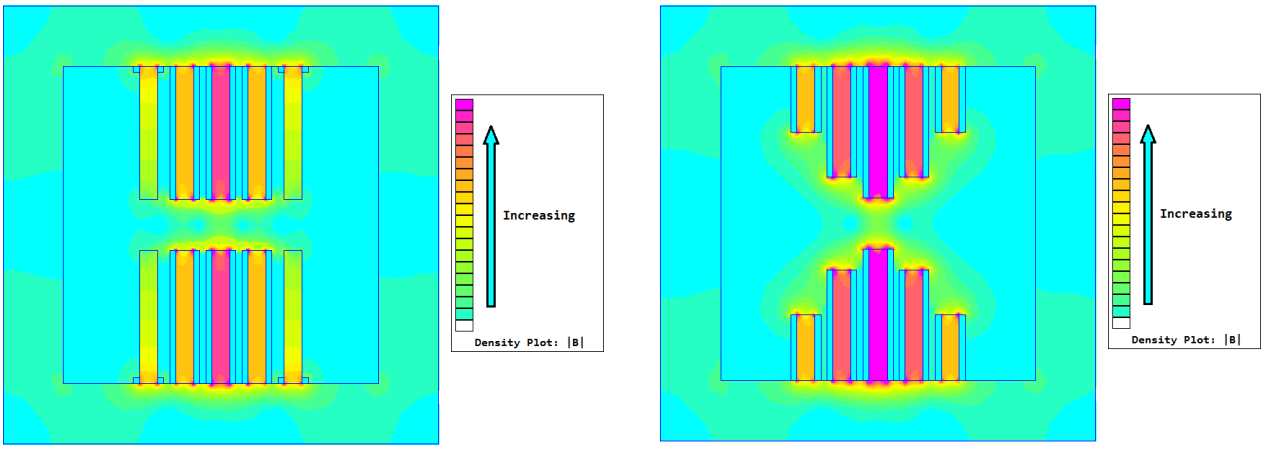

(a) (b)

Figure 27: Relative flux densities in (a) MMF optimised system and (b) gap-length optimised system

Since the main pole always has the highest flux density, it will be the first section of the machine to saturate. The relative permeability of the pole will then resemble that of air. The reluctance of that flux path will therefore drastically increase. However, the magnetic shields will ensure that the flux will stay confined to the pole area. Due to the increased reluctance, the central peak in the magnetic field intensity along the measurement line will drop relative to the peaks caused by the focus poles. The magnetic flux density for a typical scenario in which the main poles have saturated is shown in Figure 28.

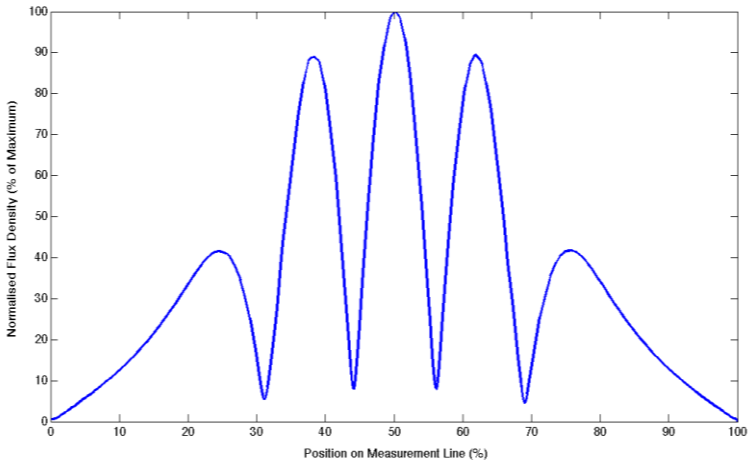

Figure 28: Focussing pattern after main pole saturates but before focusing poles begin to saturate.

If the relative MMFs, in either the MMF optimised system or the gap length optimised system, are further increased to a point at which the focus poles begin to saturate, the peaks on the measurement line will begin to decrease due to the increase in reluctance in the respective flux paths. This continues to occur until all the poles have saturated fully and all the poles have a relative magnetic permeability equal to that of air. At this stage, the output looks very similar in shape to the output pre-saturation, since the magnetic shields are forcing all the flux to remain it its proper place. The image in Figure 29 shows a visualisation of the different stages of saturation. At the front of the plot, none of the poles are saturated. When the main poles saturate, the peaks in magnetic flux density caused by the focus poles become significantly larger relative to the peak caused by the main poles, as explained above. As the focus poles begin to saturate, the peaks caused by the focus poles begin to shrink again relative to the peak caused by the main poles. If pushed far enough, all the poles will saturate and the flux density along the measurement line will resemble the initial, unsaturated field pattern. This is shown in Figure 30.

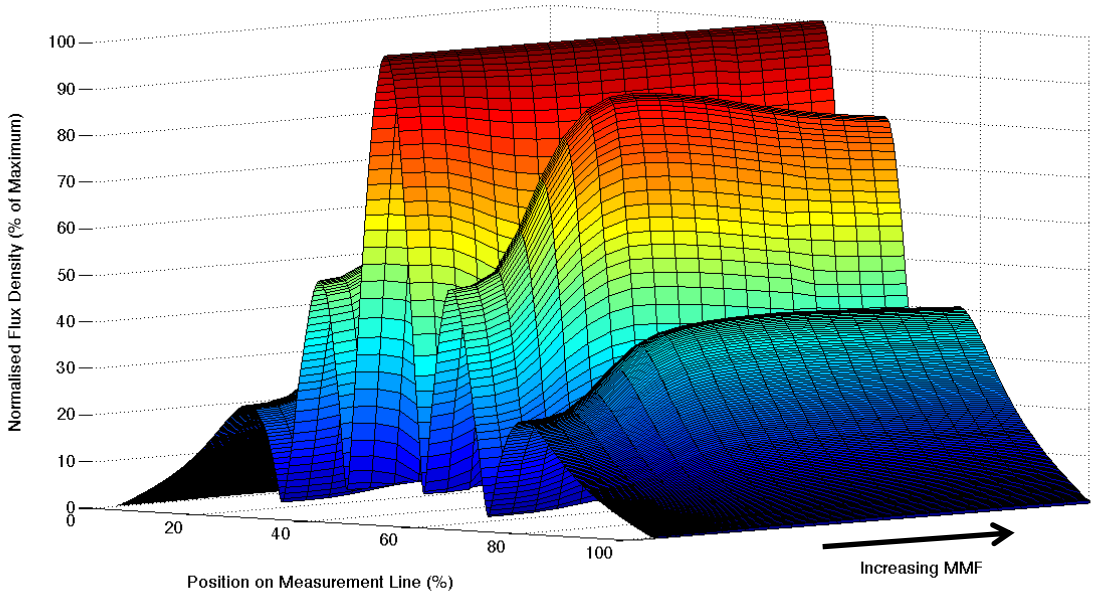

Figure 29: 3 dimensional plot showing transition from unsaturated machine behaviour to saturated machine behaviour

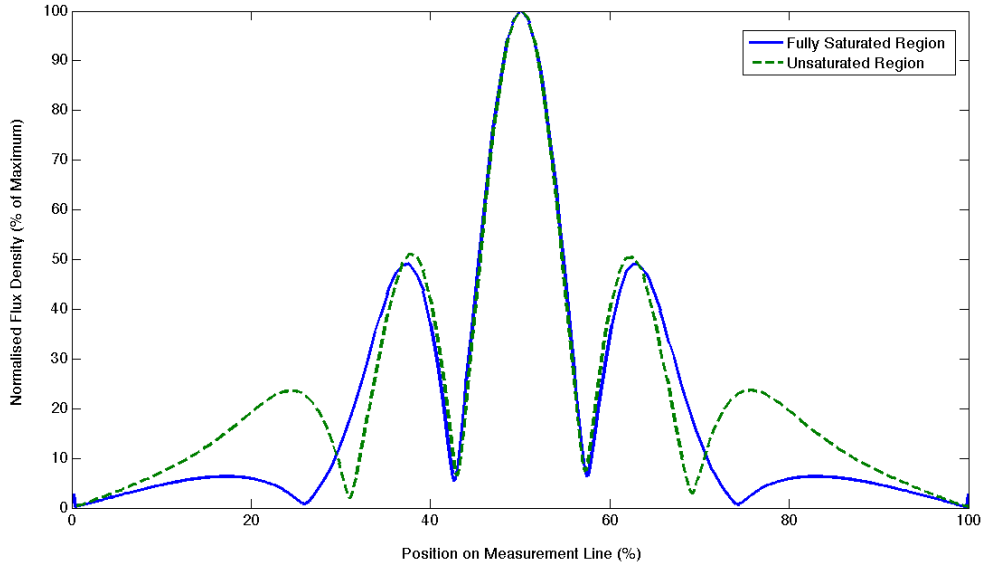

Figure 30: Plot showing similarity between the focussed fields in the unsaturated and fully saturated cases

The slight discrepancy between the field shape pre-saturation and post full saturation can be accounted for by noting that no shields were used for the second set of focus poles. Therefore, when saturation occurs, the length of the area to which the flux in the second set of focus poles is confined is greatly reduced.

This section demonstrates that the proposed machine design can be operated in different regions. In order for the peaks caused by the focus poles to remain within the pre-defined limits, the machine must either be operated in the region before saturation occurs or in the region when full saturation of all the poles occurs. It is interesting to note that if operating in the saturated region, the field amplitude in the centre of the machine can be increased without limit whilst maintaining the focussed effect, so long as sufficient MMF is available. Additionally, if operating the machine in this way, it becomes unnecessary to use a ferrite material for the poles, since air poles will work equally well.

3.9. ADAPTING THE DESIGN TO A REALISABLE PROTOTYPE

For the building of the prototype, copper shields replaced the superconductors. Copper foil sheets were used for the windings for each pole. The foil sheets ran the length of the poles. By Lenz's law, eddy currents induced in the foil sheets by flux from a neighbouring pole produce an EMF that would oppose the flux that induced them and prevent the flux from crossing the copper foil (i.e. the copper shields). This mechanism is described in chapter 2 of this dissertation. The greater the

thickness of the copper shields, the more effective they become. If the total thickness of all the copper in-between the poles is greater than the skin depth at the frequency being used, the copper shields perform almost identically to the superconducting shields in this application. The benefit of using the shields, as well as the performance of the copper shields compared to superconductor shields is shown in Figure 31.

Figure 31 was obtained by simulating the field intensity, H, at the centre of the prototype machine (described in chapter 4) as well as the corresponding average flux density, B, in the main pole of the machine. The resulting H versus B graph can be used to interpret the amount of energy required in order to get a certain level of output.

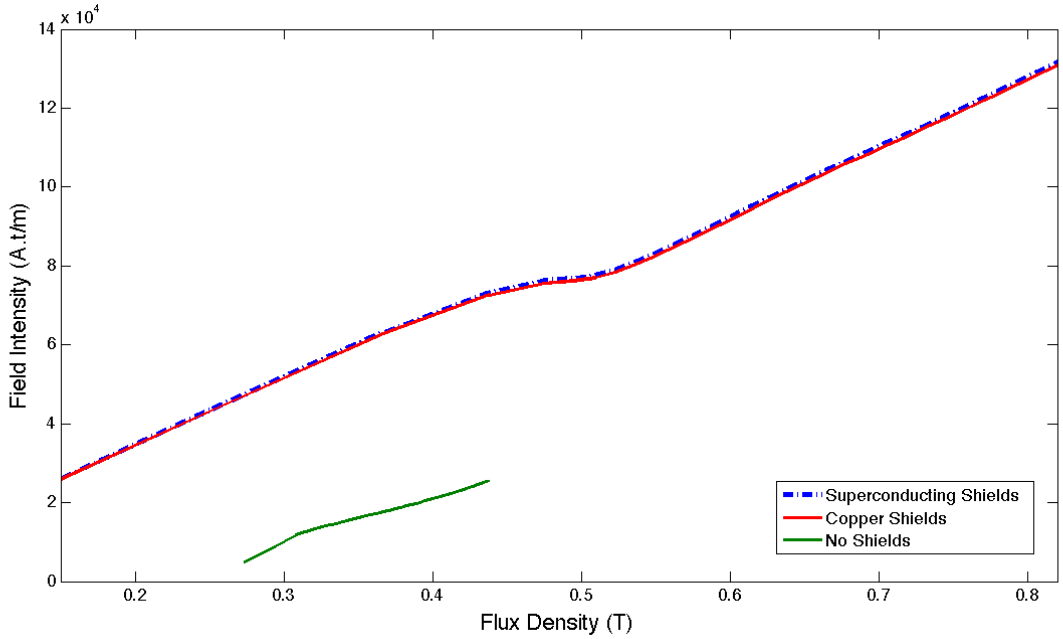

Figure 31: Plot showing the improvements in efficacy resulting from the use of shields as well as the efficacy of copper shields relative to the superconducting shields.

3.10. CONCLUSION

Focussing of a magnetic field in the very near field but at a point a small distance away from the field applicator is a new problem. As a result, no studies or other attempts to achieve suitable focussing were found in the literature. Previous investigations of coil design for hyperthermia (e.g. [2]) attempt to produce large, uniform fields. A novel method for achieving the focussing was developed and a design procedure was formulated. It was found that there exists a trade-off between

the fringing distance and the H_{pole}:H_{centre} ratio. If a small fringing distance is desired, the field intensity at the machine's pole face will be significantly larger than that at its centre. This effect was quantified and included in the design procedure. The design procedure was used in the development of a small scale system for experimental verification. This is discussed in the next chapter.

REFERENCES

[1] Hergt R., Dutz S., *Magnetic particle hyperthermia – biophysical limitations of a visionary tumour therapy*, Journal of Magnetism and Magnetic Materials, Germany, 2007.

[2] Stauffer P.R., Sneed P.K., Hashemi H., Phillips T.L., *Practical Induction Heating Coil Designs for Clinical Hyperthermia with Ferromagnetic Implants*, IEEE Transactions on Biomedical Engineering, January 1994.

[3] Serway R.A., Jewett J.W., *Physics for Scientists and Engineers*, 6th Edition, Brooks Cole, 2003

[4] Atkinson W.J., Brezovich I.A., Chakraborty D.P., *Usable Frequencies in Hyperthermia with Thermal Seeds*, IEEE Transactions on Biomedical Engineering, January 1984.

[5] Smith R J., Dorf R C., *Circuits, Devices and Systems*. John Wiley & Sons, New Jersey, fifth edition, 1992.

Chapter 4

Experiment, Results and Discussion

4.1. INTRODUCTION

In the previous chapter, a design procedure for a machine to focus a magnetic field was formulated and presented. The design procedure was formulated using two-dimensional FEA. This technique makes certain assumptions such as an infinitely deep model. As a result, it is important to verify the machine design by building a prototype machine and taking measurements in the laboratory. If the measured results show good agreement with the output predicted by the FEA, the design procedure is validated and other configurations produced by the same procedure can be trusted to perform as predicted. This chapter attempts to verify the predictions from the design procedure.

4.2. MACHINE CONSTRUCTION

4.2.1. Design

A scale machine was designed such that its construction could make use of readily available materials. This constraint limits the number of available configurations to only those with pole widths and lengths easily obtainable with common ferrite components. Owing to the difficulty in obtaining materials with specific dimensions, the machine design was carried out using the MMF approach (see chapter 3) in order to limit the large variety of poles with different dimensions required by the gap-length approach. All poles are therefore identical in their dimensions.

The machine was constructed using several pieces of material, as shown in Figure 32, in which each enclosed block is a separate piece of ferrite. The return path, i.e. the frame of the machine (shown in blue), was constructed using two ferrite I-cores per side. Each pole (shown in red) was the longest side of a ferrite E-core. Before construction could commence, the legs of the E-core were removed and the remaining side was ground flat. This configuration produced an air gap very similar to that required by the design guidelines outlined in chapter 3.

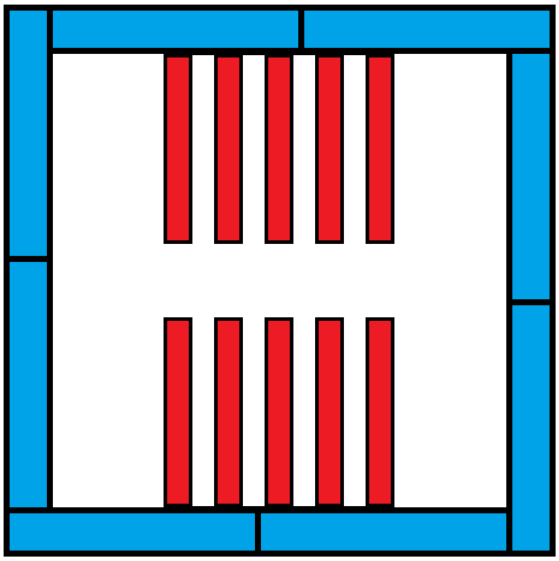

Figure 32: Arrangement of ferrite components in the construction of the prototype machine. I-cores are shown in blue. Modified E-cores are shown in red. Machine dimensions are discussed below.

Figure 33 and Table 2 show the dimensions of the machine constructed for the experiment. By applying the design guideline formulated in chapter 3, the ratio of required pole MMFs to achieve optimal focussing are approximately 5:3:1. The magnitude of the main pole MMF must therefore be five times as large as the magnitudes of the MMFs of the outermost focus poles (FP_2). Similarly, the magnitudes of the MMFs of the first set of focus poles (FP_1) must be three times larger than those of the outermost focus poles (FP_2).

Table 2: Dimensions of various parameters of the prototype machine

	Size (mm)	Size (%)
Inner Core Width	157	100
Pole Lengths (a)	65.6	41.8
Pole Widths (w)	9	5.7
Pole-to-pole separation distances (w)	9	5.7
Air Gap Length (l)	25.8	16.4
Depth	27	17.2

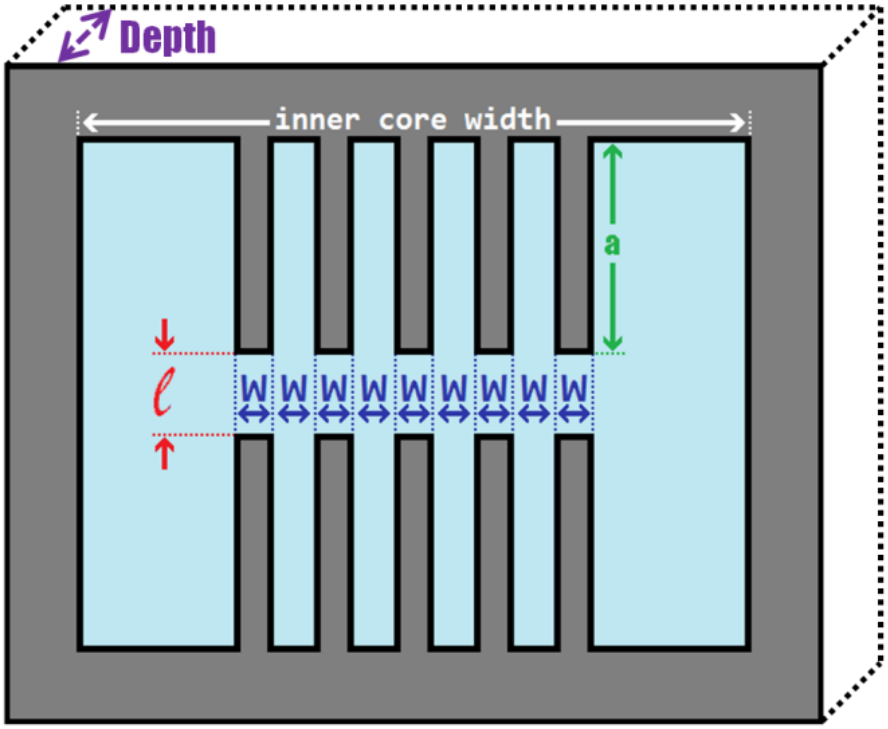

Figure 33: Drawing of machine with labelled parameters

4.2.2. Assembly

4.2.2.1. Ferrite Materials

The machine operates with an alternating magnetic field. By its very nature, the alternating magnetic field produces losses resulting from the heating of the core by the induced eddy currents. Additionally, eddy currents in the core and their associated magnetic fields would alter the focussing pattern along the measurement line. For these reasons, the machine was constructed using ferrite materials, which reduce the formation of eddy currents to negligible amounts.

The ferrite pieces were assembled as shown in Figure 32. Care was taken to ensure that the machine was adjustable should alternate configurations be required. This meant that the pieces could not be permanently bonded together. Instead, a nylon frame was constructed to securely hold the structure in place for the duration of the experiment. A photograph of the assembled structure, held together by the nylon frame, is shown in Figure 34.

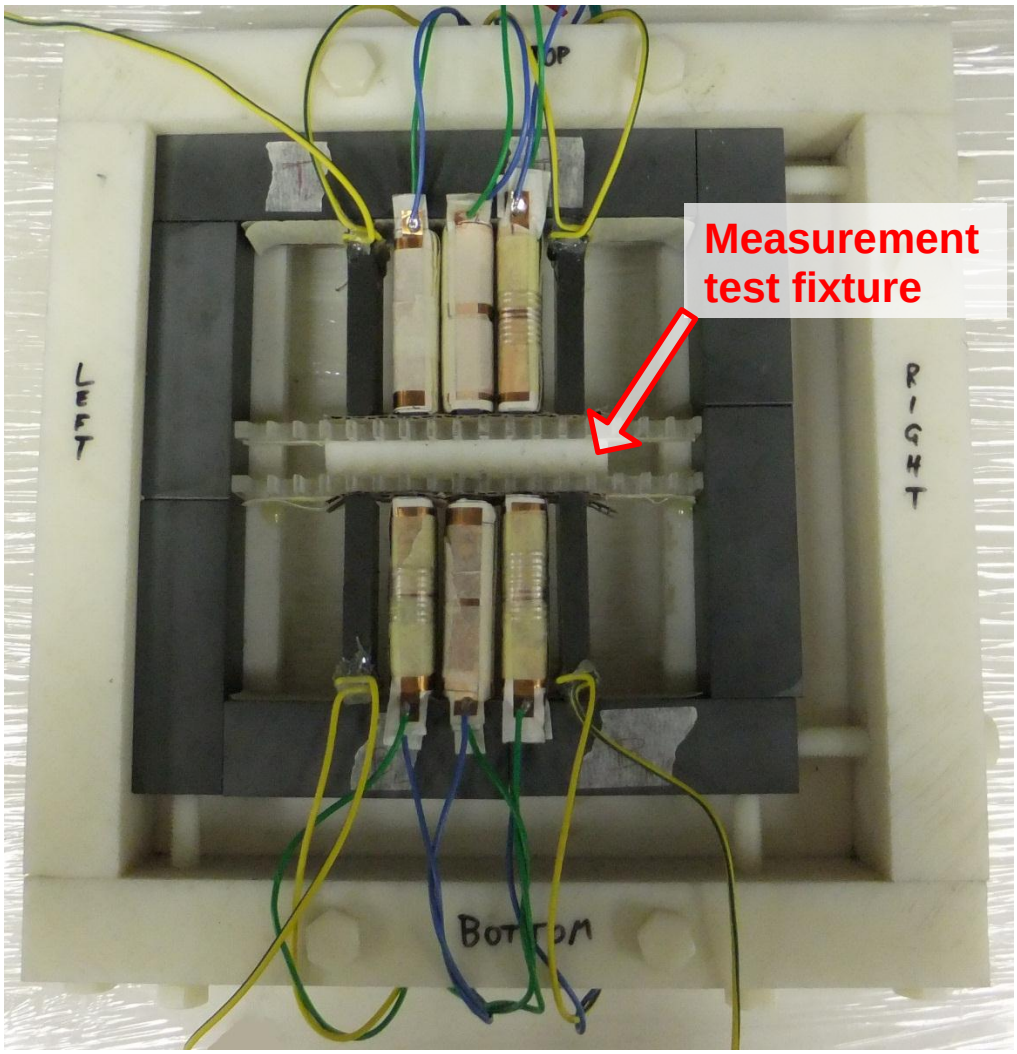

Figure 34: Fully assembled prototype machine. Ferrite pieces are held securely in place by the nylon frame.

4.2.2.2. Current Carrying Turns and Magnetic Shields

As mentioned in section 4.2.1 of this chapter, the $MMF_{main\text{-}pole}$:$MMF_{focus\text{-}pole\text{-}1}$:$MMF_{focus\text{-}pole\text{-}2}$ ratio was 5:3:1. This could easily be achieved using standard wire twisted around the pole the required number of times. Instead, however, copper foil was used along the full length of the pole. The copper foil served dual purposes. Firstly, the copper was wound the appropriate number of times around each pole and carried the required current. It was therefore responsible for setting up the MMF for each pole. Additionally, the multiple layers of copper foil occupying the space in-between the poles (i.e. in the pole-to-pole separation distance) acted as the magnetic shields as explained in section 3.9 of chapter 3. Figure 35 shows one of the poles being wrapped in copper foil. Thin paper was placed in-between each turn of the copper foil to insulate the turns from one-another.

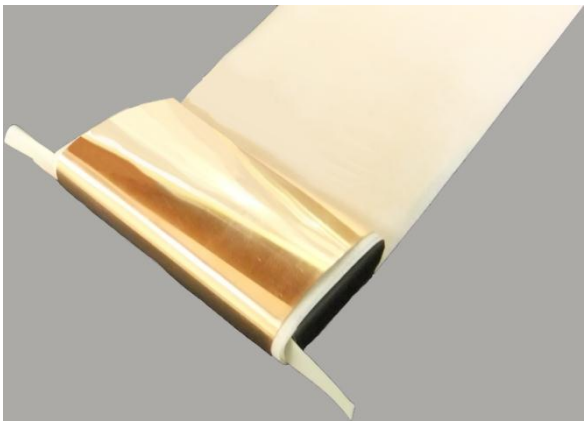

Figure 35: Pole being wrapped in copper foil. Paper is placed between each layer to insulate the turns.

4.2.3. Predicted Machine Behaviour

Figure 23 (chapter 3) can be used to predict the behaviour of the machine shown in Figure 34. The expected fringing distance is approximately 4.5% of the inner core width i.e. 7 mm. The expected focussing pattern, i.e. the plot of the simulated magnitudes of B along the measurement line, is presented in the section 4.5 of this chapter.

4.3. DRIVING ELECTRONICS

The power supply required to energise the machine must perform two tasks. Firstly, it should convert an input to a frequency suitable for AEH. A frequency in the range of 400 kHz to 500 kHz is used, as discussed in chapter 1. Secondly, the power supply must drive a current, through the coils, that is sufficient to energise it to a level at which beneficial hyperthermia treatment can be achieved. For the small-scale experimental model, this high level of machine excitation is not required, since the objective of the experiment is simply to validate the design procedure and the predicted behaviours described in chapter 3. However, a small excitation such as that from a function generator was considered too low to properly evaluate the system. A resonant power supply was therefore developed.

4.3.1. Circuit

A half-bridge, series resonant converter circuit was used to power the machine. This topology is simple to design and construct and was more than capable of supplying sufficient power to the machine for experimental purposes. The circuit diagram of the converter is shown in Figure 36.

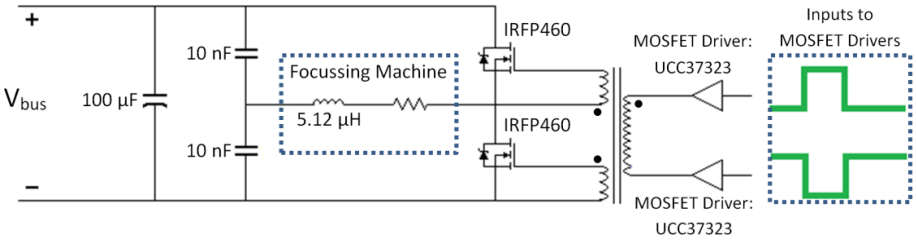

Figure 36: Circuit diagram of resonant power supply.

The circuit in Figure 36 can be analytically reduced into a series RLC circuit. The simplified circuit is shown in the right hand side of Figure 37. Current flow for the different MOSFET states is also shown.

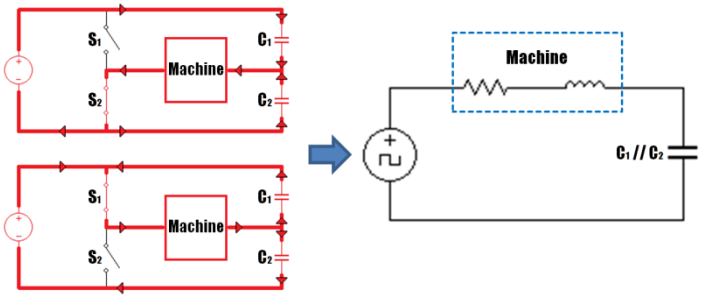

Figure 37: Reduction of resonant power supply (left) into simplified, series RLC circuit (right). The MOSFETs from Figure 36 have been drawn as switches. In the top left image, switch S_1 is open and S_2 is closed. In the bottom left image, switch S_2 is open and S_1 is closed.

4.3.2. Design Considerations

4.3.2.1. Operating Frequency

Besides for the importance of the machine excitation frequency for therapeutic hyperthermia, the frequency is also a particularly important parameter in the design and construction of the driving electronics. It is essential to ensure that the capacitors used in the circuit are rated for the specific frequency and current. Additionally, in a resonant circuit, the components are selected to provide maximum power transfer at a specific resonant frequency.

4.3.2.2. Resistive Load

The real component of the load in the heating system arises from losses in the machine itself as well as the losses in the particles within the tumour. However, the combined mass of the particles within the tumour is very low since there is a limit on the concentration of particles that can be used without causing toxicity or a dangerous reduction of hepatic reserve. Since the losses are directly

related to the mass of the particles, the losses in the particles can be neglected at the supply. This does not imply that the losses are insignificant to the patient i.e. the losses in the particles may be sufficient to achieve therapeutic heating of the tumour. However, the losses in the particles as seen by the supply can be considered negligible when compared to other losses in the machine.

4.3.2.3. Stray Inductance

The circuit inductance should arise from the coils in the machine. However, at useful frequencies, stray inductance from the wiring becomes significant. It is therefore recommended that an effort be made to minimise unnecessary long lengths of wires and remove any loops of wires that are not required. The wiring in the experimental system was carefully connected such that stray inductance was minimised.

4.3.2.4. Power Capacitors

The power capacitors used in the resonant circuit are subjected to a large potential difference across their terminals. For this reason, the capacitors must be chosen to be able to withstand the high voltages and currents at the required frequency. The capacitors used in the experiment meet this criterion.

4.3.2.5. Switching Components

The frequency range of 400 kHz to 500 kHz is important in choosing the components for the oscillator section of the circuit. This frequency range is above the limits for certain components such as most IGBTs. MOSFETs are able to switch fast enough, carry sufficient current and withstand the high potential differences that exist in the power supply. MOSFETs are therefore used in the oscillator section of the circuit.

The half bridge rectifier requires two switches i.e. two MOSFETs. The control circuitry, responsible for switching the MOSFETs, consists of two MOSFET drivers with outputs connected to a gate drive transformer. The transformer then applies out-of-phase square waves to the gates of the MOSFETs. This can be seen in Figure 36.

4.3.3. Impedance

The machine was wired as demonstrated by Figure 38. All of the turns around the top sets of poles (shown in red) were wired in series with each other. Similarly, all of the turns around the bottom sets of poles (shown in blue) were wired in series with each other. A parallel connection was then made between the two sets of series connections (shown in purple).

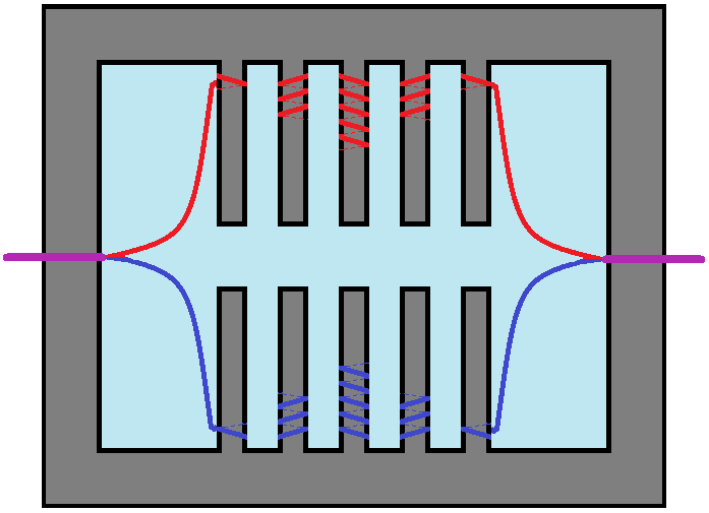

Figure 38: Wiring of the prototype machine.

The inductance of the machine was measured at the ends of the parallel connection (shown in purple). The measured inductance was 5.12 µH. This inductance could then be used to identify the required capacitors for the system to operate at resonance in the desired frequency range. This is achieved by making use of equation 4.1.

$$2\pi f = \frac{1}{\sqrt{LC}} \qquad (4.1)$$

Where L is the inductance of the machine, C is the capacitance of the required capacitor and f is desired, resonant frequency. This frequency was chosen to be 500 kHz. From equation 4.1, it was found that approximately 20 nF of capacitance was required for $C_1//C_2$ (Figure 37). This means that 10 nF capacitors would be used for C_1 and C_2, as shown in Figure 36.

4.4. MEASUREMENT SENSOR

A search coil was used to obtain measurements of flux density (B) at multiple, equally spaced points along the measurement line. An EMF is produced at the terminals of the search coil, which can be measured using an oscilloscope. From these measurements, the flux densities can be calculated.

4.4.1. Physics

Equation 4.2 arises from Faraday's law of magnetic induction.

$$\varepsilon = -N \frac{d\phi}{dt} \qquad (4.2)$$

where ε is the induced EMF and $\frac{d\phi}{dt}$ is the rate of change of magnetic flux with respect to time.

Furthermore, it is known that the flux term in equation 4.2 can be rewritten in terms of flux density and loop area. If the flux is sinusoidal, this results in equation 4.3.

$$\varepsilon = -NA \frac{d(B \sin 2\pi f t)}{dt}$$

$$= -2\,\pi\, f\, N\, A\, B \cos(2\pi f t) \qquad (4.3)$$

The maximum value of the cosine term in equation 4.3 will be unity. Since measurements will be taken using the magnitude of the peak values of EMF, measured EMFs will be related to the peak flux density as shown in equation 4.4.

$$|\varepsilon_{max}| = 2\,\pi\, f\, N\, A\, B_{max} \qquad (4.4)$$

4.4.2. Construction

The sensor coil was constructed using 0.22 mm copper wire with an enamel coating. Eleven turns were wound around a hollow, plastic ring. A second layer of ten turns was then added making a total of twenty-one turns. The mean diameter of the turns was 5.55 mm. This results in a measurement area of 24.2 mm^2 i.e. the sensor can measure the average magnetic flux density over this surface area. All materials in the sensor can be considered to have permeabilities equal to that of free space (i.e. $\mu_r = 1$). The probe is therefore negligibly field perturbing.

4.4.3. Calibration

Much care was taken to ensure the reliability of the measurements taken using the sensor. In order to verify the sensor's accuracy, a calibration chamber was constructed and used to calibrate the sensor. The calibration chamber consists of two identical coils arranged to form a Helmholtz coil. The purpose of the calibration chamber was to provide a homogeneous, predictable magnetic field to verify the accuracy of the sensor and to determine a scaling factor to be used to correct all future measurements. The sensor is shown in the calibration chamber in Figure 39.

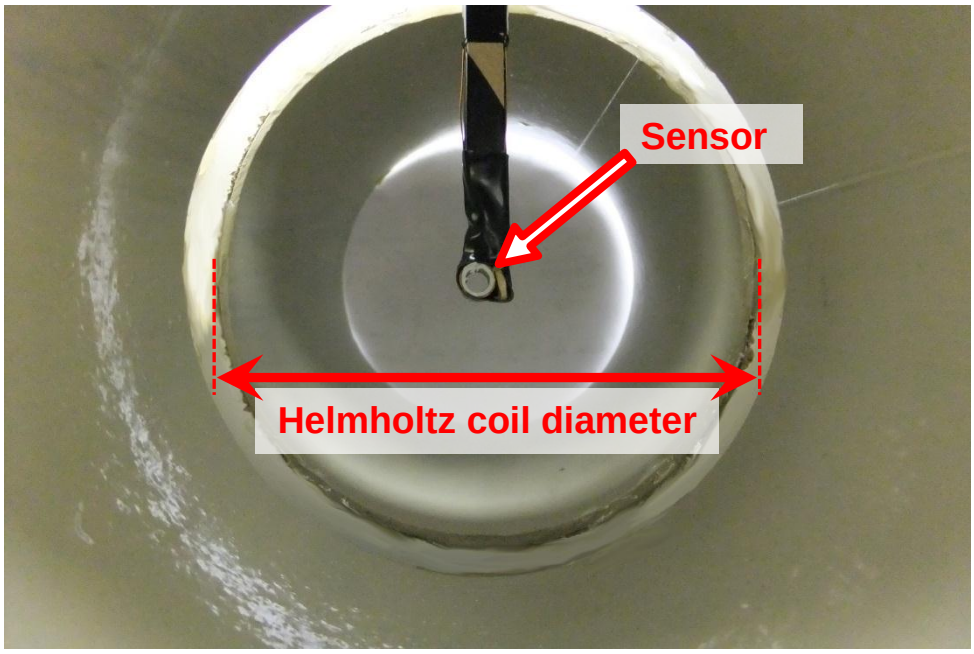

Figure 39: Sensor in calibration chamber.

4.4.3.1. Helmholtz Coil

The Helmholtz coil consisted of two identical, circular coils, each made up of 300 turns of copper wire. The coils had a mean radius of 52.5 mm and were therefore spaced 52.5 mm apart. Equation 4.5 can be used to accurately calculate the flux density inside the Helmholtz coil [1].

$$B = \mu_0 \times \frac{0.7155\, N\, i}{r} \qquad (4.5)$$

where r is the radius of the coils and *i* is the current flowing in the turns of the coils.

The Helmholtz coil can be used with either an AC or DC input. A direct current source of 1 A was used to energise the calibration chamber. For the specific Helmholtz coil, with 1 A flowing in the coils, the magnetic flux density should be marginally larger than 5 mT. A professionally calibrated gaussmeter was used to verify the correct functioning of the calibration chamber at DC excitation. A correct reading from the gaussmeter provided confidence that the Helmholtz coil was functioning correctly.

4.4.3.2. Calibration Results

The calibration chamber was energised using a 50 kHz supply. This was the upper end of the frequencies that could be achieved, without distortion resulting from saturation occurring with the equipment available in the laboratory. The peak current flowing through the coils was measured to be 4 mA. The measurement sensor was placed within the calibration chamber and the voltage across its terminals was measured on a high accuracy multimeter.

The ratio between the accurate, calculated flux density and the measured flux density from the measurement sensor was 0.924:1. This suggests that measurements obtained using the coil sensor should be multiplied by a scaling factor of 0.924 in order to improve the measurement accuracy. It should be noted that this scaling factor is expected to be constant for all frequencies, i.e. even though the experiment was performed at a frequency significantly higher than 50 kHz, the scaling factor remains the same.

The discrepancy can be attributed to wire thickness and other non-ideal issues arising from the construction of the sensor.

4.5. RESULTS AND DISCUSSION

The measurement sensor was fastened to a jig designed to move the sensor into 49 equally spaced regions along the measurement line. The terminals of the sensor were connected to a probe attached to an oscilloscope. At each position, the maximum value of the sinusoidal output was recorded. The recorded EMFs were used to calculate the corresponding flux densities using equation 4.4. The final experimental results were obtained by multiplying the flux densities by the scaling factor obtained using the Helmholtz coil (as described in section 4.4.3.2 of this chapter).

The final measured values of flux density were overlaid on top of the focussing curve predicted by FEA. This is shown in Figure 40.

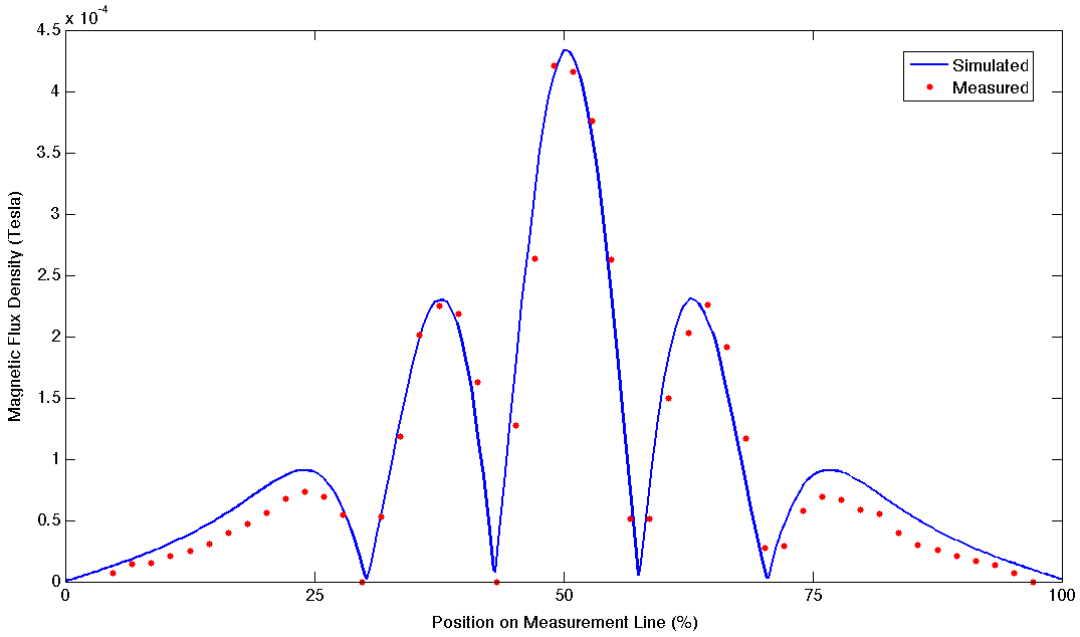

Figure 40: Expected flux densities along the measurement line as predicted by FEA (solid blue line) and measured flux densities along the measurement line (red dots). Each red dot marks a measured value.

The measured values correspond very well with the simulated focussing pattern. This is especially true at the peaks caused by the main poles and the inner most focus poles (FP_1). The maximum values of these peaks match up with the simulated values with good agreement. Additionally, the field attenuates to zero in-between peaks just as predicted by the simulation.

There is a slight discrepancy between the measured and simulated values towards either end of the machine i.e. the measured values of the outermost peaks are slightly lower than expected. This can be attributed to the difference in the infinitely deep model used by the simulation and the finite thickness of the machine constructed for the experiment.

This difference is noticed towards the ends of the measurement line because the distance between the outermost sets of poles (FP_2) and the machine frame is large relative to the thickness (or depth) of the physical machine. The flux from the outermost poles therefore fringes in the third dimension i.e. in the dimension that the simulation treated incorrectly. This can be seen in Figure 41. The flux from the outermost poles occupies a greater area than predicted, resulting in a reduction in flux density.

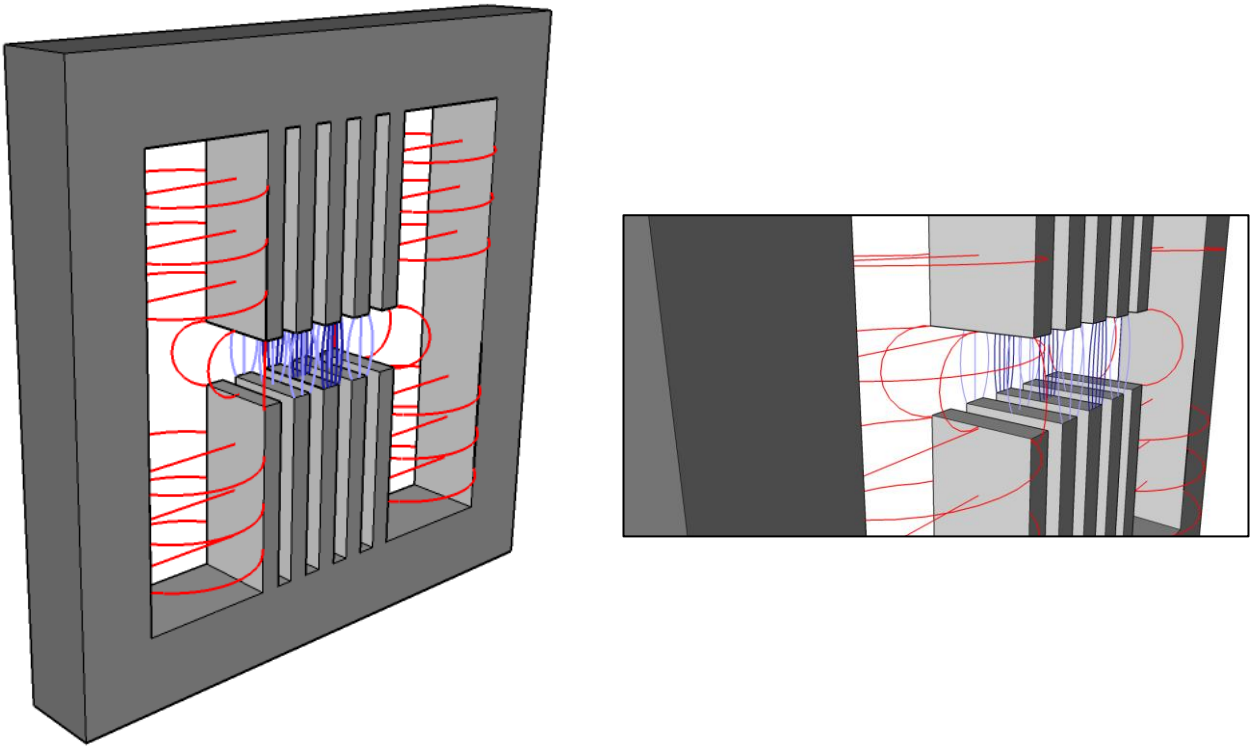

(a) (b)

Figure 41: (a) Three dimensional drawing of prototype machine. (b) Enlarged, angled view of flux in the centre of the machine. Fringing flux from the outermost sets of focus poles is shown in red.

4.6. CONCLUSION

It has been shown that there is very good agreement between the simulated and measured values. The slight discrepancy between the results towards either end of the measurement line has been accounted for and has little effect on the performance of the machine. This result gives confidence in the design procedure from chapter 3, since the predicted behaviour corresponds well to measurements obtained using a prototype machine. This suggests that the simulations are accurate representations of the physical machines. This produces confidence that all simulated results are equally accurate, including those of other configurations as well as of the H_{pole}:H_{centre} ratios.

REFERENCES

[1] Jiles D. *Introduction to Magnetism and Magnetic Materials*. Taylor & Francis Group, Florida USA, second edition, 1998.

Chapter 5

Recommendations for Future Work and Conclusion

5.1. RECOMMENDATIONS FOR FUTURE WORK

5.1.1. Medical Hyperthermia Treatment

This research provides an improvement in the technology responsible for producing the magnetic field in various MMH treatment modalities. Much modelling is required in order to assess the level of usefulness of the focussed magnetic field applicator for different tumour types and locations. In order to perform this modelling, detailed knowledge of the particle characteristics would be required. This is briefly discussed in chapter 2. Additionally, it would be essential to correctly capture the thermal conductivities of the cells in the body. Cooling mechanisms such as perfusion would need to be taken into account. Finally, animal testing would be required before approval for a full scale clinical trial would be granted.

5.1.2. Closed Form Mathematical Solution

It was seen in chapter 3 that adding poles to the machine introduced additional peaks in field amplitude when measured along the focussing line. The additional peaks were constrained to be lower in amplitude than the main peak. Similarly, the gap length of the additional poles was larger than that of the main pole. This relationship suggests that there may be an analytical solution to obtaining a design procedure for the magnetic field focussing applicator. This solution may be found by using Fourier techniques to analyse space harmonics.

5.1.3. Other Applications

5.1.3.1. Integrity Verification for Distant Items

Magnetic fields may be used to locate problems in the integrity of a physical device or structure. There may be a case where the device or structure is out of reach or blocked. Typical magnetic field applicators would produce significant fringing if they were used at a distance, for this purpose. This would result in inaccurate measurements. A single sided version of the machine designed in chapter 3 could cancel out the fringing flux and improve the accuracy of these measurements. A single sided device is a version of the machine from chapter 3 with just the top sets of poles. An example

of a device, for which this could be useful, is a vessel with many layers of thermal padding. The thermal padding may create a significant distance between the measurement device and the vessel.

5.1.3.2. Metal Detection

Magnetic fields are used by metal detectors to find conductive materials beneath a surface. The penetration of the field is dependent on the surface as well as the frequency of the field. In some cases, a particularly penetration depth may be required. However, at lower frequencies, the accuracy obtained may be insufficient. A focussed magnetic field may provide a solution to this problem as it would increase the accuracy of the apparatus, even at reduced frequencies.

5.2. CONCLUSION

Background information for existing MMH technologies have been presented in chapter 1. Included in this is a discussion of the problems facing other researchers in the field. The method by which this research attempts to overcome these problems is introduced and explained.

Before an in-depth analysis of the problem could be discussed, it was necessary to review some theory regarding the physics of magnetism and of magnetic materials. These topics were covered in chapter 2. Knowledge of magnetic materials is vital in understanding how losses result in the heating of the materials, thereby producing hyperthermia in the tumour cells. Furthermore, a detailed understanding of magnetic phenomena allowed for the exploitation of these phenomena in order to achieve the desired focussing.

Chapter 3 describes, in detail, the parameters that influence the focussing of a magnetic field. Physical constraints were discussed and trade-offs were made. An in-depth analysis of the results from many simulations gave rise to a design procedure, by which the complicated design of the focussing apparatus was greatly simplified using graphs. This is the primary contribution of this work. The focussed magnetic field is a novel technique for improving the results of MMH.

The final chapter describes how a prototype system was constructed to validate the design procedure. The system consisted of a small scale focussing machine as well as driving electronics in order to provide sufficient electrical excitation to the machine. The design and construction of the small scale prototype, the electronics and the measurement sensor is documented. The experiment was performed and measurements were obtained. These measurements were then compared to results predicted by simulations. The measured results were in good agreement with the predicted results. The slight discrepancy towards either end of the measurement line resulted from fringing

caused by the finite depth of the real machine, which was not taken into account by the simulation. The good agreement validates the design procedure and suggests that all models designed using the procedure, as well as all parameters discussed, would perform as expected.

In order to fully understand the contribution of this work, it is necessary to comprehend the magnetic theory regarding the loss mechanisms of the particles to be supplied to the tumour (as described in chapter 2). The loss mechanisms available in MMH combined with a magnetic field within the safety limits (discussed in chapter 1), are not alone capable of providing a feasible alternative to other cancer treatments. An improvement in the efficacy of MMH would arise from the use of a focussed magnetic field instead of the commonly used homogenous magnetic field. This research provides a method for achieving large thermal losses in a small region of an organ infused with magnetic particles. Using this research, it is possible to achieve the high magnetic field intensity within the tumour region required to cause necrosis of the tumour cells. By using the design procedure from chapter 3 to create the machine and rotating the machine relative to the patient, it may be possible to produce the required heating within the tumour without damaging the surrounding, healthy tissue.

Much work remains before the hyperthermia system can find its way into hospitals. This is discussed in the section on recommendations for future work. However, a novel contribution to the field of MMH has been made. Additional uses for a focussed magnetic field have also been discussed, such as in integrity verification and metal detection.

Appendix A

Design Curves for Single Focus Pole and Triple Focus Pole Configurations

A.1. INTRODUCTION

A design procedure for the focussing apparatus is described in chapter 3. It is shown in chapter 3 that there is an increase in performance when moving from the one focus-pole configuration to the two focus-pole configuration. Furthermore, the data shown in chapter 3 also suggests that there is little benefit to be gained from the use of more than two sets of focus poles. Therefore, the recommended design procedure makes use of the two focus-pole configuration.

However, in order to arrive at the conclusions stated above, simulations were performed for configurations with one set of focus poles, two sets of focus poles and three sets of focus poles. This appendix shows the results of these simulations. All results were obtained using the FEMM finite element analysis software package.

A.2. DESIGN CURVES

As explained in chapter 3, fringing distance is the distance taken for the magnetic field to attenuate from its maximum to 50% of its maximum (in percentage of the inner core width). Additionally, the pole width axis in each graph has been represented as a percentage of the inner core width. Pole width is always used as a design parameter because different pole widths require different configurations (MMFs or gap-lengths) in order to achieve good results.

The ratio, H_{pole}:H_{centre}, describes the ratio of the magnetic field intensity at the pole face to the magnetic field intensity at the centre of the machine. This quantity is described in detail in chapter 3.

The design curves for the configurations with one set of focus poles and three sets of focus poles are now given. Curves have been fitted to data points in Figure 42, Figure 43, Figure 46 and Figure 47 in an attempt to extract a trend. It is important to remember that a brute force optimisation procedure was used to obtain all values. This means that values were varied by fixed discrete amounts with each iteration. For this reason, error bars of length equal to the discrete steps are

included in the graphs. The trend lines were adjusted until they passed through most of the regions within the error bars.

A.2.1. MMF Optimised

Figure 42 or Figure 43 is used in order to obtain the correct relative MMFs for the focus poles for various pole widths (for the one pole set and three pole sets configurations respectively). All MMFs are relative to the MMF of the main pole.

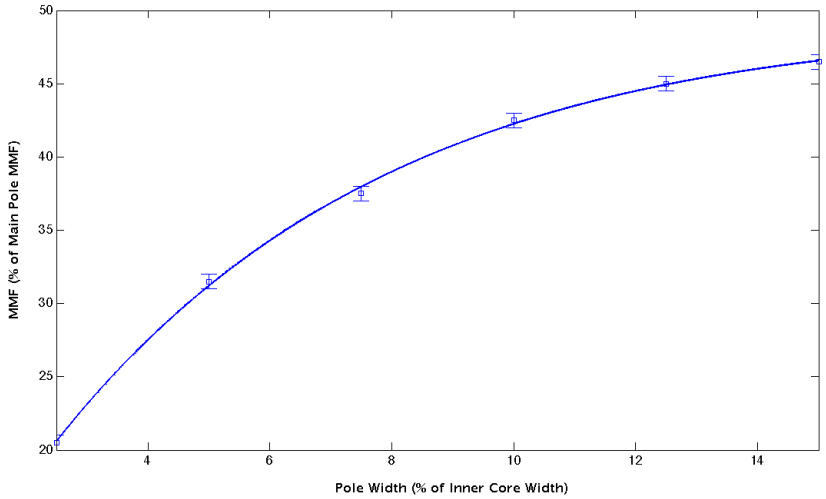

Figure 42: Relative MMFs of focus poles to achieve optimum focussing for the configuration with one set of focus poles.

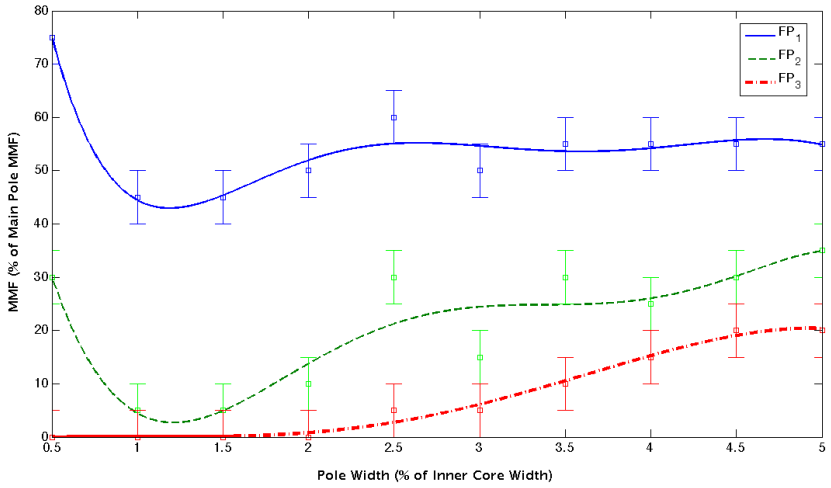

Figure 43: Relative MMFs of focus poles to achieve optimum focussing for the configuration with three sets of focus poles.

Figure 44 and Figure 45 show the fringing distance and H_{pole}:H_{centre} ratio for various pole widths, when the MMF(s) for the poles are set as suggested by Figure 42 and Figure 43 respectively.

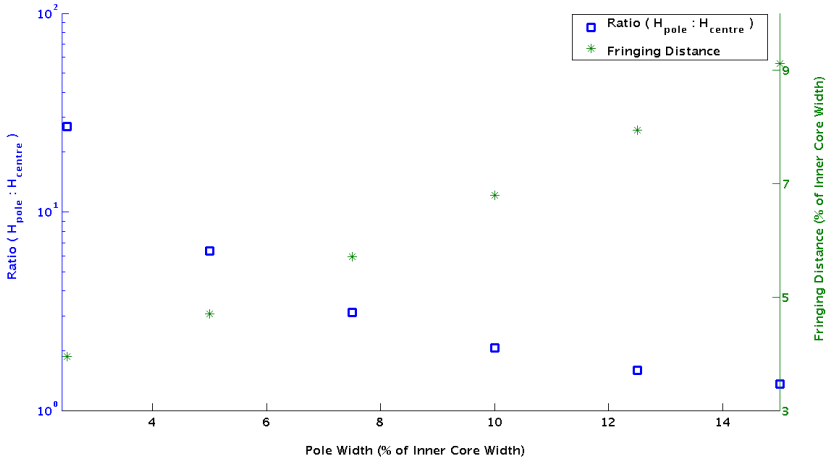

Figure 44: H_{pole}:H_{centre} ratio and fringing distance obtained when MMF applied to FP_1 is setup according to Figure 42.

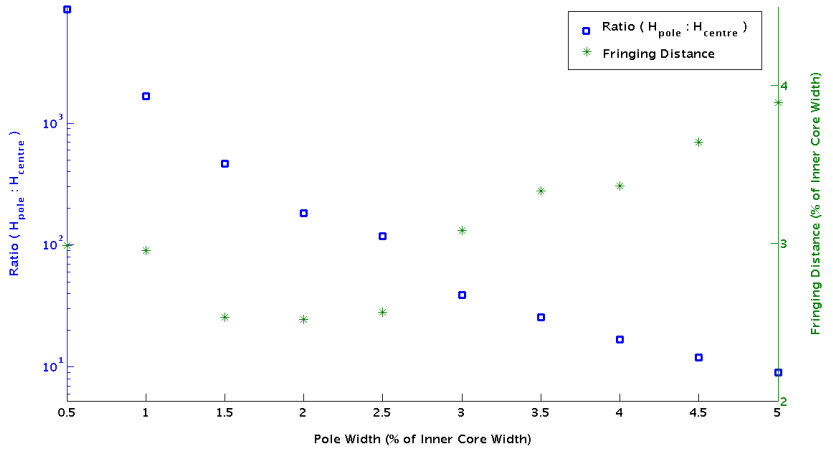

Figure 45: H_{pole}:H_{centre} ratio and fringing distance obtained when MMFs applied to FP_1, FP_2 and FP_3 are setup according to Figure 43.

A.2.2. Gap-Length Optimised

Figure 46 or Figure 47 is used in order to obtain the correct relative gap-lengths for the focus poles for various pole widths (for the one pole set and three pole sets configurations respectively). All gap-lengths are percentages of the inner core width.

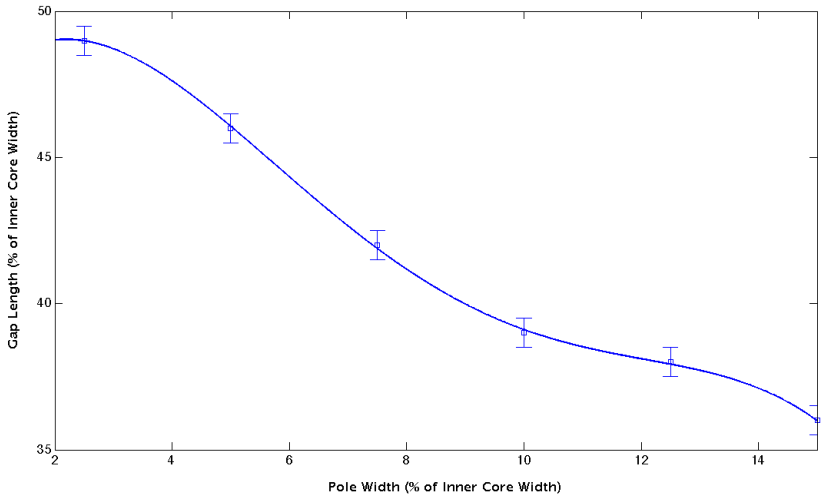

Figure 46: Relative focus pole gap-lengths to achieve optimum focussing for the configuration with one set of focus poles.

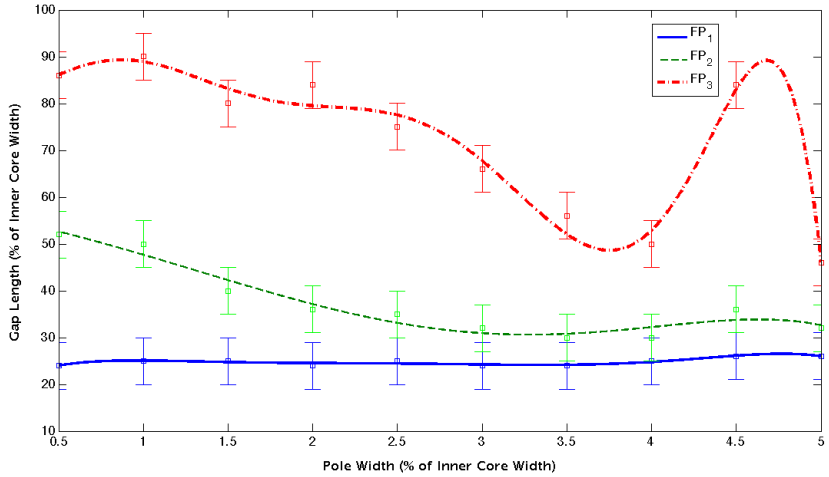

Figure 47: Relative focus pole gap-lengths to achieve optimum focussing for the configuration with three sets of focus poles.

Figure 48 and Figure 49 show the fringing distance and H_{pole}:H_{centre} ratio for various pole widths, when the gap lengths are set as suggested by Figure 46 and Figure 47 respectively.

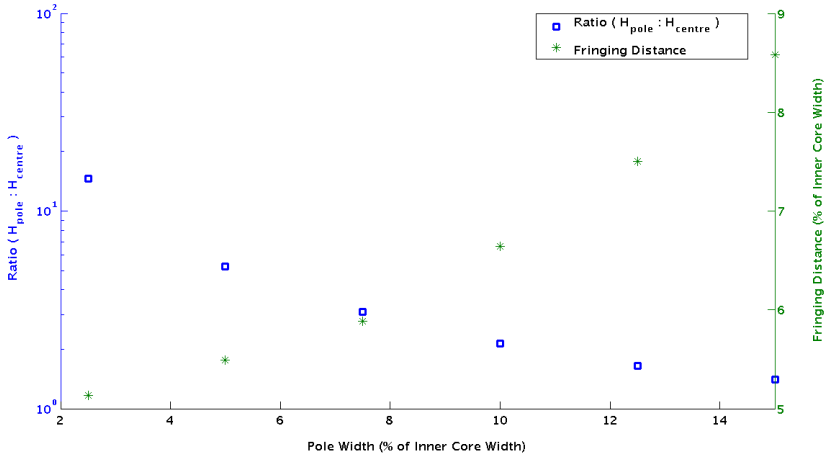

Figure 48: H_{pole}:H_{centre} ratio and fringing distance obtained when gap-lengths of focus poles are setup according to Figure 46.

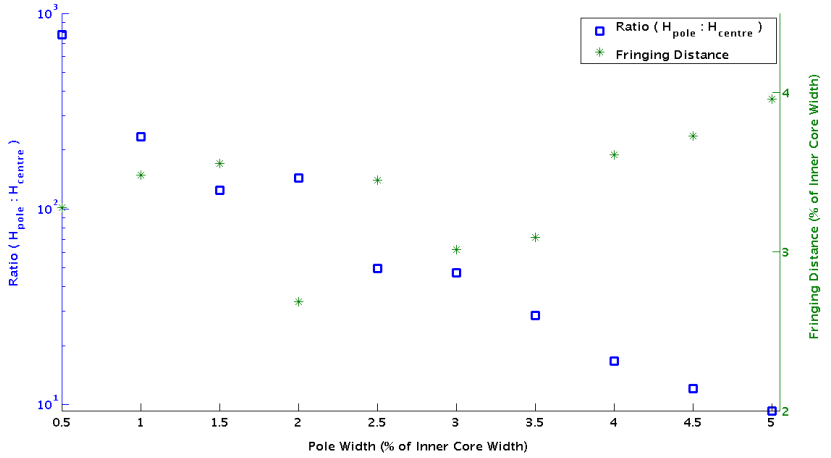

Figure 49: H_{pole}:H_{centre} ratio and fringing distance obtained when gap-lengths of focus poles are setup according to Figure 47.

A.3. CONCLUSION

It has been shown in chapter 3 of this dissertation that a configuration with two sets of focus poles produces good results with minimal complexity, compared to configurations with one set or three sets of focus poles. In order to reach this conclusion, all three configurations were investigated. This appendix presents the results from the simulations with one set and three sets of focus poles.